

Article

Submarine Manoeuvrability Design: Traditional Cross-Plane vs. x-Plane Configurations in Intact and Degraded Conditions

Benedetto Piaggio ^{1,*}, Giuliano Vernengo ¹, Marco Ferrando ¹, Giorgio Mazzarello ² and Michele Viviani ¹

¹ Department of Naval Architecture—DITEN, University of Genoa, 16145 Genoa, Italy

² Fincantieri DMM, 16129 Genoa, Italy

* Correspondence: benedetto.piaggio@unige.it

Abstract: Submarines' manoeuvrability both in intact and degraded operating conditions is the main design concern starting at the very early stages of design. This increased complexity of the design process compared to a surface vehicle can only be handled by using dynamics numerical simulations on both the vertical and horizontal manoeuvring planes. To this aim, a 6-DoF method is presented, validated, and applied to study the manoeuvring characteristics of several vessels. The analysis has been conducted considering two standpoints, i.e., to verify the design handling capabilities of the vehicles at low and high speeds and to study the off-design residual abilities in the eventual case of emergency operations with jammed/lost-control surfaces. The influence of different design features, such as, e.g., the stern plane "+" and "x" configurations, fairway size and positioning, hull dimensional ratios and restoring capabilities have been analysed in terms of impact on turning ability, course and depth changing abilities, and vertical/horizontal course stability, including the vertical damping ratio and critical velocity.

Keywords: submarines; underwater vehicles; manoeuvrability; stern planes; rudder; design

Citation: Piaggio, B.; Vernengo, G.; Ferrando, M.; Mazzarello, G.; Viviani, M. Submarine Manoeuvrability Design: Traditional Cross-Plane vs. x-Plane Configurations in Intact and Degraded Conditions. *J. Mar. Sci. Eng.* **2022**, *10*, 2014. <https://doi.org/10.3390/jmse10122014>

Academic Editors: Md Jahir Rizvi and Apostolos Papanikolaou

Received: 21 October 2022

Accepted: 6 December 2022

Published: 16 December 2022

Publisher's Note: MDPI stays neutral with regard to jurisdictional claims in published maps and institutional affiliations.



Copyright: © 2022 by the authors. Licensee MDPI, Basel, Switzerland. This article is an open access article distributed under the terms and conditions of the Creative Commons Attribution (CC BY) license (<https://creativecommons.org/licenses/by/4.0/>).

1. Introduction

State-of-the-art dynamic manoeuvring simulations are made of prediction methods built with a modular structure cross-combining semiempirical, numerical, and experimental data gathered within historical dataset knowledge. Considering surface vessels, there are plenty of references dealing with such approaches for single-screw vessels [1–6], twin-screw vessels with either traditional [7–11] or podded propulsion systems [12–14], and working vessels [15–17]. Parallely, the scientific community is increasingly focusing on the direct system identification for autonomous surface shipping applications [18–20] from free-running tests, eventually combining the approaches of the CFD-RANSE methods [21]. Starting from the MMG framework by Kose and Ogawa [22,23], different approaches have been developed, focusing on the IMO manoeuvring design goals [24]. On the other hand, while fewer methods are available in the literature to assess the manoeuvring characteristics of underwater vehicles, there is a complete lack of modular regression models and comparative campaign matrixes useful for design purposes.

Considering Munk theory [25] initially developed for airships and torpedoes [26], different approaches foster relatively simple methods for assessing the manoeuvring capabilities of submarines, mainly treating them as simple ellipsoidal shapes or only including the appendages in terms of stability and controllability derivatives. Indeed, different from surface vehicles, submarine hydrodynamics should be studied in 6-DoF by splitting the horizontal and vertical planes' manoeuvring performances to enable the identification of many terms. While there is no particular difference with respect to surface

vehicles on the horizontal plane aside from the stern-dipping phenomenon or the surface proximity effect, vertical plane manoeuvring prediction requires additional design considerations due to the pitching restoring moment caused by the vertical misalignment of the centre of gravity with the centre of buoyancy [27]. These effects on the handling of the vehicle need an additional positional dependency term independent from the vessel speed to the set of equations, thus increasing the order of the ODEs involved. As a result, the complexity of the directional stability analysis on the vertical plane rises, becoming speed-dependent and introducing the possibility of both oscillating convergent behaviours and/or divergent solutions. Then, thanks to the speed dependency, from a design perspective, the vertical sailing stability at a constant depth, the eventual damping factor of the oscillations, and the depth-changing controllability are turned into additional requirements. Indeed, the stern planes may become ineffective in keeping control of the sailing depth when operating below a critical velocity. The sail or bow planes are typically installed to overcome this problem in lower speed ranges to best apply the vertical force near the neutral point, i.e., the longitudinal centre of pressure of the vessel sailing with an angle of attack—for full details see Appendices A and B.

Within this framework, the mostly applied semiempirical methodology that meets the demand of a linear manoeuvrability assessment is the so-called AEW approach [28]. This approach has been developed for submarines showing a cross-plane rudder configuration only, splitting the hull, fairway, and control plane contributions separately while including their mutual interactions. This methodology addresses the amplification or loss of effectiveness of the control surfaces when mounted onto the ellipsoid hull or trunk of cones, such as in the case of the stern planes and rudders. The interaction effects are then divided into two components: a body-on-wing contribution and a wing-on-body one [29]. Particular focus is given to the effects of the vortex shed by the fairway tip on the hull lifting capabilities and the consequent upper stern plane inflow angle modification. This method is suitable to assess the manoeuvring performances over straight sailing, providing a comprehensive analysis of the vessel's stability and controllability but accepting very small perturbations around the linearization point. Consequently, such a model is not adequate for full nonlinear manoeuvres, such as turning, harsher dynamic zigzag testing, and fast emersions emergency operations.

On the other hand, a standardized mixed analytical nonlinear form of equations was laid out by Feldman and Gertler [30,31] and Bohlmann [32], suiting the towing tank captive model testing experience. The latter revised model encompasses classical linear terms with the addition of semiempirical nonlinear modelling arising from the crossflow drag theory in the direct and cross-planes of motions. Its most peculiar feature is the inclusion of an out-of-plane stern-dipping term due to the shedding of the sail tip vortex when horizontally drifting, plus an additional unsteady effect: This vortex, in fact, induces a crossflow along the hull which breaks the symmetry of the hydrodynamic pressure field between the deck and keel. The control plane models are kept within a linear framework. The resultant wide and complex analytical form of the equations needs to be fed a large computational (RANSE) and/or experimental captive model testing (CMT) dataset. However, determining the whole sets of coefficients is not a practicable option for parametric design studies.

Some authors have dealt with this problem by using, e.g., CFD-RANS methodologies to evaluate fully appended hydrodynamics [33–36] for tailfin sizing [37], the effectiveness of tailplanes mounted onto hulls [38,39], and the vortex structures shed onto the tailplanes [40]. More recently, some authors exploited the possibility of coupling dynamic simulation models with RANSE methodologies [41,42] to assess cross-plane vs. x-plane designs [43,44] to study highly unsteady rising manoeuvres with consequent roll instabilities [45] or for the analysis of manoeuvring at periscope depth [46]. Finally, the system identification approach of submarine dynamics from free-running model tests [19,47,48] supplies a powerful and complementary approach to the proper settling of

simulation models when combined with historical EFD knowledge and CFD methodologies.

There are two largely used public benchmark case studies that are the so-called DARPA Suboff, for which experimental captive model tests are available [49], and the newer BB2 submarine, for which free-running tests have been performed [50]. Most of the studies specifically address these two geometries, but almost none of them aim to evaluate the effect of the variation of different design parameters on the manoeuvrability characteristic of the vessels.

In this perspective, a manoeuvrability prediction method has been developed combining the AEW approach, Gertler model, and experience developed at the Department of Naval Architecture of the University of Genoa (DITEN) on surface ships into a new dynamic simulation model capable of capturing the main effects with a reduced number of terms. This model has been validated and used to compare different submarine design configurations.

In particular, three submarine designs presented in Section 2 have been extensively studied. The modelling approach is described in Section 3.1, and the validation both in terms of a captive model and free-running tests are shown in Sections 3.2 and 3.3, respectively. Finally, the developed method is used as a design tool for a submarine configuration. The reference design intact condition is described in Section 4.1, including the effect of the variation of different design features, such as the stern plane “+” and “x” configurations, fairway size and positioning, hull dimensional ratios, and restoring capabilities. The speed dependency analysis is presented in Section 4.2, and the analysis in degraded conditions is then shown in Section 4.3.




2. Case Studies

The selected benchmark fleet was made of the three submarines shown in Table 1. The DARPA Suboff is a model scale research submarine from the Defence the Advanced Research Projects Agency (DARPA) Suboff project at the David Taylor Research Centre (DTRC) where captive model tests have been carried out [49]. The simple vehicle geometry is widely acknowledged to be unrealistic (the fairwater is too small, the torpedo is a simple revolution body, and it has small stern planes and no bow control surfaces) and course unstable. Very few attempts of manoeuvre simulation have been done, resulting in a large spread of results due to its strongly unstable property [51,52]. The second vessel, called the SWE, is a demo submarine from the Swedish navy [53]. Results of captive and free-running model tests are available even if there is no reference; these data come from numerical simulations or experimental tests. The third one, called the SMG, is a real but decommissioned submarine, according to which both captive model tank tests and full-scale manoeuvres are available. These results are reported in this work, but the geometry is confidential.

The selected vessels are described in more detail in Table 1 in terms of nondimensional ratios. The main particulars of the hull, fairwater, and control planes are referred to as the bare hull longitudinal area projected onto the vertical plane (A_v) and the horizontal plane (A_h). In particular, the rudder and stern plane characteristics, indicated by the subscript ‘r’ and ‘s’, respectively, refer to the + or x configuration to the percentage of movable control area over the fin area, the total fin area over the vertical and horizontal projected areas of the hull (A_r/A_v and A_s/A_h), and the percentage of the hull-projected trunk area. The latter can either be A_t/A_r or A_t/A_s ; the trunk is indicated by the subscript ‘t’, the portion of the hull radially included between its longitudinal symmetry axis and the root of the considered fin. The ratio A_t/A_s plays a key role in terms of increasing the body-on-wing effectiveness and as an amplification factor of the wing-on-body effect. The same quantities were evaluated for the fairwater, indicated by the subscript ‘f’, and for the bow-panes, indicated by the subscript ‘b’. The location with respect to the midship is indicated as a percentage of the length of the vessel. The SWE

and SMG submarines rely on + and x stern plane configurations, respectively, and are representative of a modern and realistic class of submarines.

Table 1. Submarines—case studies.

		DARPA	SWE	SMG	
					
Hull	L/B	8.57	10.05	9.66	-
	B/Ht	0.70	0.47	0.54	-
	Ht/H	1.44	1.55	1.53	-
Fairwater	position	24	22	12	%
	Af/Av	4.5	9.1	9.0	%
	At/Af	110	96	100	%
Stern planes	type	+	x	+	-
	position	-40	-42	-42	%
	movable	100	100	100	%
	2×Ar/Av	2.6	$2 \times 3.2 \times \cos 45^\circ = 2 \times 2.3$	2.5	%
	At/Ar	120	64	87	%
	movable	100	100	60	%
	2×As/Ah	2.6	$2 \times 3.8 \times \cos 45^\circ = 2 \times 2.7$	5.0	%
	At/As	120	64	50	%
Bow planes	position	24	25	12	%
	movable	100	100	100	%
	2×Ab/Ah	1.6	2.0	2.2	%

3. Description of the Mathematical Model

The simulation approach used relies on a 6-DoF modular MMG-inspired model [2,22] suitable for design purposes with ad-hoc developed parametric design options. The contributions from the bare hull, the appendage system, and the propulsion and control means were split, considering their mutual interactions and according to the canonical Newton equations as described by Bohlmann [32] and Feldman [31]. A summary of the breakdown modelling is presented next.

A standard reference system was adopted for the vehicle, i.e., centred amidship along the longitudinal axis passing through the propeller centre, as displayed in Figure 1a. Considering that the vehicle induced velocities at specific location $[u_R, v_R, w_R]$, several local reference systems were introduced, e.g., at each control surface, to evaluate the in-plane reference velocities *chord-wise* ahead of c_o , *span-wise* out of s_o to the tip, and perpendicularly in the *thickness-wise* t_o direction according to the right-hand rule, as shown in Figure 1b. The stern planes were numbered from one to four from the vertical lower rudder and moving in a clockwise direction if looking from the stern according to the mounting angle Γ . The methodology provided the lift L and drag D for the generically installed control plane by assessing the chord-wise and thickness-wise inflow velocity within the plane section itself according to the resultant velocity V_R and effective angle of attack δ_e , as shown in Figure 1b. The resultant \tilde{X} and \tilde{Y} forces were finally projected onto the vehicle reference according to the mounting angle rotation.

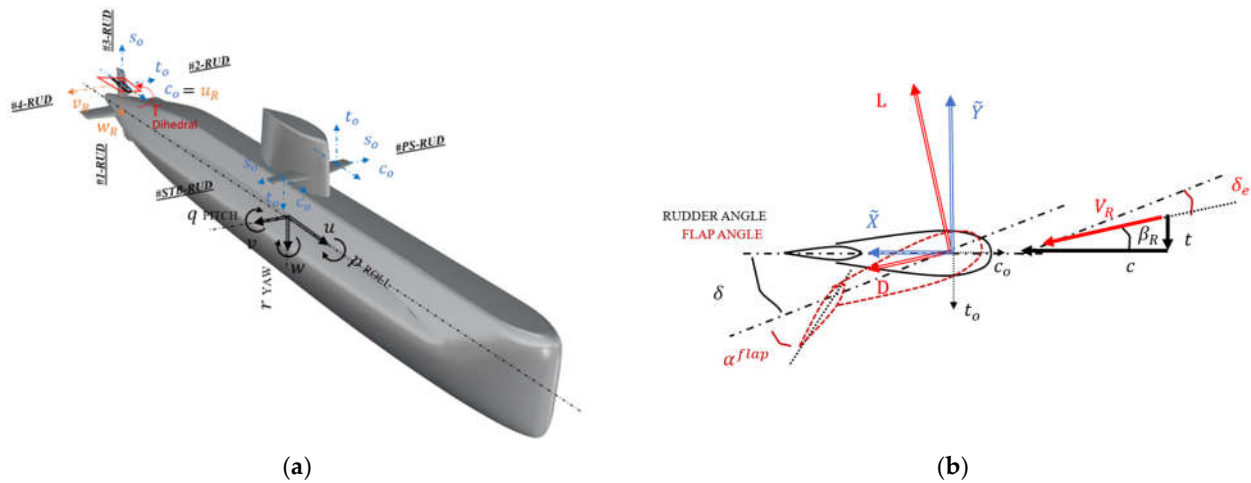


Figure 1. Reference systems. (a) Vehicle kinematics. (b) Control planes definitions.

3.1. Modelling

Bare Hull. The linear lift and nonlinear crossflow drag of the bare hull were predicted in the framework of a strip theory-based approach, relying on slender body sectional theory as fostered by Clarke [53] and later by Bohlmann [32]. More details can be found from Toxopeus [54] and Piaggio [14]. According to this approach, the hull shape was defined by transverse sections. The forces were divided into linear components based on slender body theory including real-fluid corrections for the uv and ur terms and into a fully viscous nonlinear contribution that relies on quadratic crossflow drag theory.

Such a method is able to encompass arbitrary sectional shapes by using simple ellipsoids forms with two-dimensional added mass formulations. Figure 2 sketches the sectional approach where each section accounts for a contribution of forces and moments on the horizontal plane. By including viscous corrections, this methodology allows for a bow–stern unbalancing of forces according to the potential Munk theory.

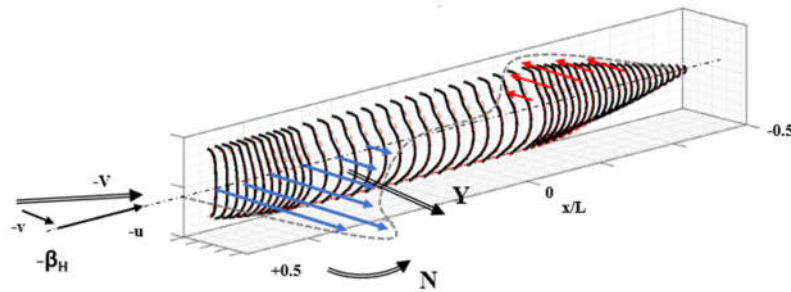


Figure 2. Bare hull—strip theory sectional forces.

From the 2D sectional added masses, linear properties at the generic section at the coordinate ξ were assessed on the horizontal and vertical planes according to the following equations:

$$\begin{aligned}
 m_{yy}(\xi) &= \frac{1}{2} \rho \pi H(\xi)^2 C_H(\xi) \\
 m_{zz}(\xi) &= \frac{1}{2} \rho \pi B(\xi)^2 C_V(\xi)
 \end{aligned}
 \tag{1}$$

where $H(\xi)$ is the sectional vertical axis height, and $B(\xi)$ is the horizontal axis breadth while $C_H(\xi)$ and $C_V(\xi)$ are the nondimensional coefficients, respectively.

The 3D distribution of the forces was derived accordingly by integration from bow to stern. A viscous semiempirical correction was applied to the ideal Munk theory by modifying the added mass gradient at stern shapes [55], resulting in new distributions of crossflow due to drift and rotation. In the horizontal plane, these terms are named M_{yy}^{uv} and M_{yy}^{ur} . The linear derivatives were obtained by integration as in the following equations:

$$\begin{aligned}
 Y_{\dot{v}} &= - \int_{stern}^{bow} M_{yy}^{uv} dx & Y_{\dot{r}} &= - \int_{stern}^{bow} M_{yy}^{ur} dx \\
 N_{\dot{v}} &= - \int_{stern}^{bow} x M_{yy}^{uv} dx & N_{\dot{r}} &= - \int_{stern}^{bow} x M_{yy}^{ur} dx
 \end{aligned}
 \tag{2a}$$

$$Y_{uv} = -M_{yy}^{uv}|_{stern} \qquad Y_{ur} = -M_{yy}^{ur}|_{stern} \tag{2b}$$

$$N_{uv} = - \left[M_{yy}^{uv}|_{stern} + \int_{stern}^{bow} M_{yy}^{uv} dx \right] \qquad N_{ur} = - \left[x M_{yy}^{ur}|_{stern} + \int_{stern}^{bow} M_{yy}^{ur} dx \right] \tag{2c}$$

Classic crossflow drag formulations were considered to include the nonlinear effects for large kinematics according to the horizontal and vertical crossflow velocities locally induced by the vehicle’s motions at each section:

$$\begin{aligned}
 v(x) &= v + rx \\
 w(x) &= w - qx
 \end{aligned}
 \tag{3}$$

For instance, in the horizontal plane, the nonlinear contribution was obtained through the integration of the sectional contributions according to the following equations:

$$\begin{aligned}
 Y_{cfd} &= -0.5\rho \int_{stern}^{bow} C_{Dh}(x) v(x)|v(x)| H(x) dx \\
 N_{cfd} &= -0.5\rho \int_{stern}^{bow} C_{Dh}(x) v(x)|v(x)| H(x) x dx
 \end{aligned}
 \tag{4}$$

where $C_{Dh}(x)$, the horizontal crossflow drag sectional distribution, was evaluated according to semiempirical 2D formulations as a function of the breadth over height section ratio B/H and the sectional coefficient C_x . The same method was applied on the vertical plane.

Appendages. The fairwater (sail), bow planes, and stern planes/rudders contributions account for the hull sectional geometry on which they are mounted. In particular, the mutual interaction effects may be distinguished into two counterparts [28,56]: the *body-on-wing* effect, i.e., an increase in the effective aspect ratio with respect to the isolated fin (tip-induced downwash), and the *wing-on-body* interaction, i.e., an amplification of the forces due to an extension of the fin pressure fields onto the hull part below.

Starting from the isolated fin, the hydrodynamic modelling might include a spade, horn/skeg, and flap features. Lift and drag formulations were developed according to experimental evidence $\frac{dC_L^o}{d\alpha}$, stall, and post-stall hydrodynamics by varying the following parameters [57–60]:

- Effective Aspect ratio “ ar_e ”;
- Taper ratio “ λ ”;
- Sweep angle “ Λ ”;
- Tip shape “ τ ” (squared or faired);
- Thickness ratio “ t/c ”;
- Horn percentage “ A_{horn}/AR ”;
- Flap percentage “ A_{flap}/AR ”.

As far as the hull mounting interaction is concerned, given the generic pair of fins mounted on the elliptical or circular section, the total wingspan was defined as the full extent in between the fin tips, including the (imaginary) part of the bluff body in between the roots of the fins, as shown in Figure 3, given the installation angles of Figure 4. Such an additional part has a dimension r , and the resultant wingspan is $b = 2(r + s)$. Considering the exposed control surface area, $A = cs$, the upper bound of the effective aspect ratio is $ar_e = b^2/A_e$, where A_e is the effective planform area. Given the span s and mean chord c , the isolated lift slope $\frac{dC_L^0}{d\alpha}$ of the fin was evaluated according to:

$$A_e = A + cr$$

$$ar_e = \frac{(s + r)^2}{A_e} \tag{5}$$

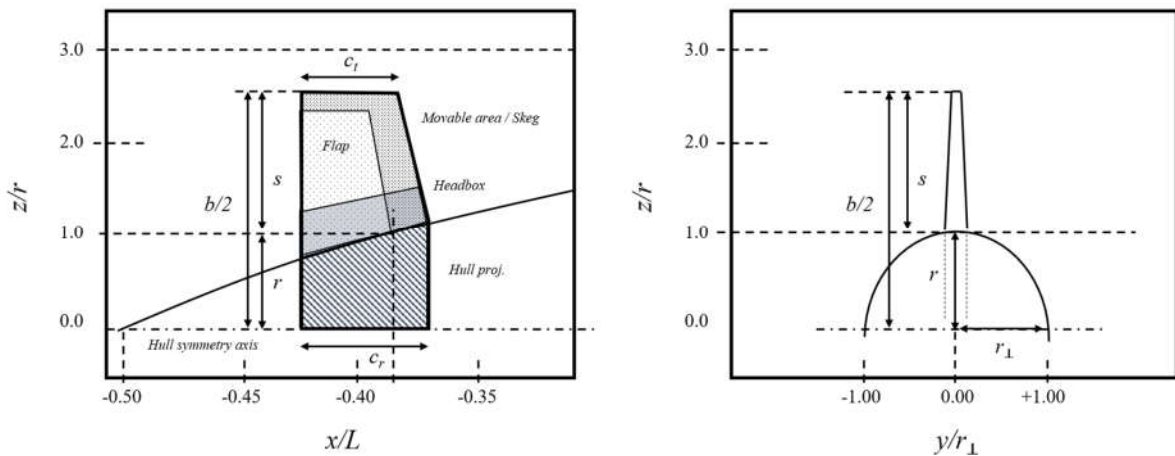


Figure 3. Control surfaces geometry.

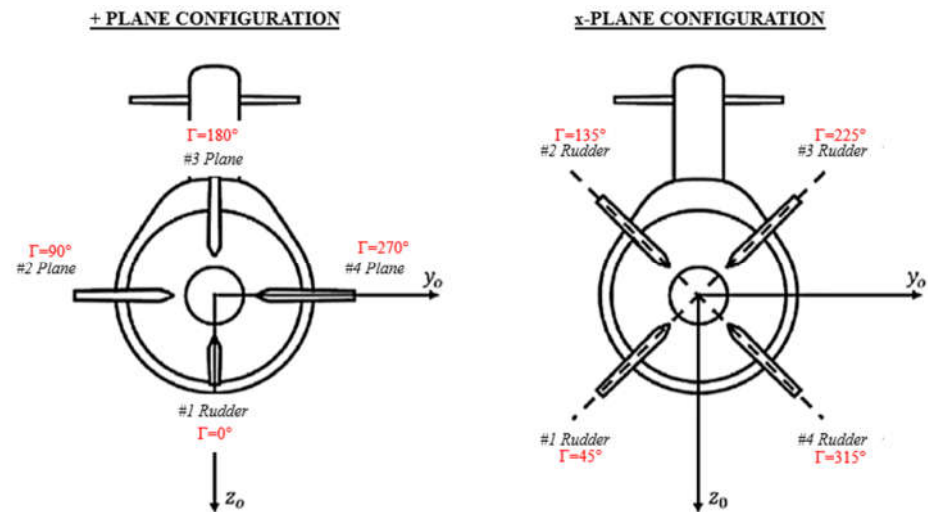


Figure 4. Stern control surfaces—configurations.

The circulation effectiveness should then be diminished due to the fact that the imaginary, additional part of the effective wing is a bluff geometry. Moreover, the body will share a part of the fin load but in a smaller amount due to its relative size and curvature with respect to the fin. Ideally, with a radius of curvature that tends to be infinite, the body will not perceive any amplification as it would with a wall-mounting wing (solid mirror plane effect) with the consequence of a doubly effective aspect ratio.

On the contrary, with a radius of curvature that tends to zero, the wing becomes the direct union of the two isolated fins, as they should be joined at their root, again, with zero amplification on the body.

Considering the linear slope coefficient of the whole effective projected planform $\frac{dC_L^o}{d\alpha}$, the interactions were considered separately for the stability and controllability features of the vessel [29]. In terms of stability, i.e., fixed fins or movable planes but with zero geometric angles, the two interactions were included within the coefficients $K_{b(w)}^*$ and $K_{w(b)}^*$, as shown in Figure 5. In terms of controllability, a loss of effectiveness was experienced due to the gap opening at the root of the planes when a nonzero geometric angle of the plane was set. This can be assessed according to two analogous terms $k_{b(w)}$ and $k_{w(b)}$, as shown in Figure 6. Then, an efficiency decay term in controllability γ_δ was evaluated as a ratio with respect to the stability contribution according to the following equation:

$$\gamma_\delta = \frac{A [k_{b(w)} + k_{w(b)}]}{A_e [K_{b(w)}^* + K_{w(b)}^*]} \tag{6}$$

Consequently, the effective lift slope and angle of attack, given the geometric angle δ and local drift angle β_R and acting on the whole equivalent area A_e , become:

$$\frac{dC_L'}{d\alpha} = \frac{dC_L^o}{d\alpha} (K_{b(w)}^* + K_{w(b)}^*)$$

$$\delta_e = \gamma_\delta \delta - \beta_R \tag{7}$$

For fixed fins such as, e.g., the fairwater, a similar theory was used, as shown in Figure 7. The equivalent isolated wing was first considered, i.e., the mirrored pair of fins joined at the root for the aspect ratio according to the single fin area A . The effectiveness was then increased, and amplification was added:

$$\frac{dC_L'}{d\alpha} = \frac{dC_L^o}{d\alpha} (K_{b(w)} + K_{w(b)})$$

$$\delta_e = -\beta_R \tag{8}$$

For both the movable and fixed fins, the effective crossflow angle β_R took the hull and sail-induced wake fields into account due to the lifting bound and trailing vortexes detached. The downstream-induced velocities by the sail, in fact, broke the symmetry of the lower and upper shell flow fields both in terms of longitudinal and crossflow components, finally impinging onto the planes and rudders. According to Pattison [28], specific straightening coefficients can be introduced to correct and deteriorate the upper tail plane’s functioning with respect to the sail lift without modifying the shadowed planes with respect to the hull when drifting and rotating. With this purpose, specific cfd studies have been undertaken according to Franceschi [10] at UNIGE and will be an object of a near future publication.

Finally, the complete lift curves were obtained according to trigonometric definitions to couple the effects of both stability, due to the effective angle of attack δ_e given the local crossflow angle β_R , and control, due to the plane δ or flap angle α_f , while encompassing the stall angle [14]. In particular, the stall angle was highly anticipated due to the absence of the propeller wash benefit in terms of K_T/J^2 . In terms of drag, the contributions of the zero-angle drag, i.e., the viscous and form resistance, induced drag due to lift, and crossflow drag [60], were linearly summed. The effects of possible movable parts, such as flaps or the complementary to the fixed skeg part, were included by a shift of the curves. This was obtained with the term $\partial C_L^o(\alpha_f)$ as a function of the flap chord extension, the trailing edge geometry, and the span extension [61–63], as shown in Figure 8, and by varying the zero-angle drag $C_{Do}(\alpha_f)$:

$$C_L = \partial C_L^0(\alpha_f) + \frac{\partial C_L}{\partial \alpha} \sin \delta_e \cos^\zeta \delta_e \tag{9}$$

$$C_D = C_{D0}(\alpha_f) + \frac{C_L^2}{e \pi a r_{eff}} \cos \delta_e + c_{CFD} \sin^2 \delta_e$$

The described approach allowed for the assessment of an arbitrary stern plane configuration by evaluating the inflow components at each control surface reference system in terms of the angle of attack, absolute velocity, lift, and drag forces. The global forces in the submarine reference system were then obtained by rotating the components of force according to the local inflow angle and geometric mounting angle.

It is worth noticing that—in purely geometric and theoretical terms—the x-plane configuration exploits four planes together in terms of controllability instead of the two of the cross configuration but with a 45° mounting angle with respect to the manoeuvring plane—see Figure 4. Then, each control force should be consistently projected, i.e., with a total contribution of $4 \frac{\sqrt{2}}{2} = 2\sqrt{2}$, against the total two of the + setup. On the other hand, in terms of stability, the contributions of the +-plane and x-plane setups are geometrically equivalent. Indeed, the inflow at each plane reduces to the same angle to obtain the in-plane angle of attack. Considering the four surfaces of the x-plane setup, a total contribution of $4 \frac{\sqrt{2} \sqrt{2}}{2} = 2$ was obtained, which is equivalent to the contribution of the two vertical surfaces of the +-plane setup. Consequently—in this ideal context—the lone x-plane benefit was about $\sqrt{2}$, i.e., +40%, in controllability while it was the same in terms of stability. Nevertheless, it should be recalled that the actual functioning and effectiveness of the configurations vary depending on the interactions with the sail and the hull, as previously discussed, both in terms of wake and straightening effects. Full details will be included in the next work in progress. In addition, it should be recalled that all these considerations apply if the four identical fins are rotated at the same mounting angle. Moreover, the +-plane solution did not incur the lower rudder span limitation due to the keel line proximity. A final operative remark concerns the x-plane redundancy on both the manoeuvring planes in case of failures; this will be discussed in the next sections.

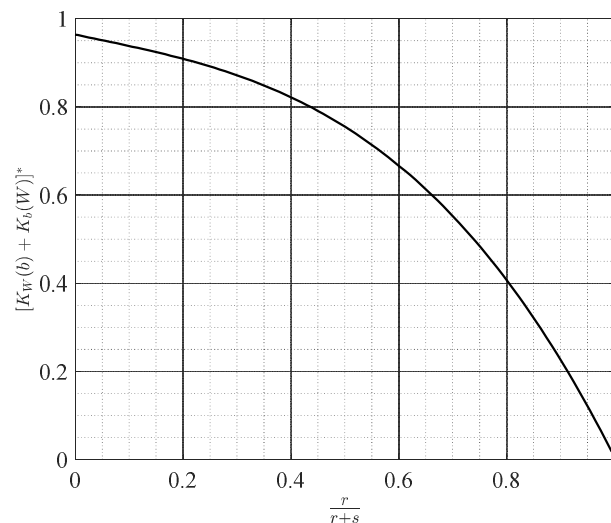


Figure 5. Stern control surface—stability loss due to fins at the tail end of hulls with respect to the full-span equivalent wing [29].

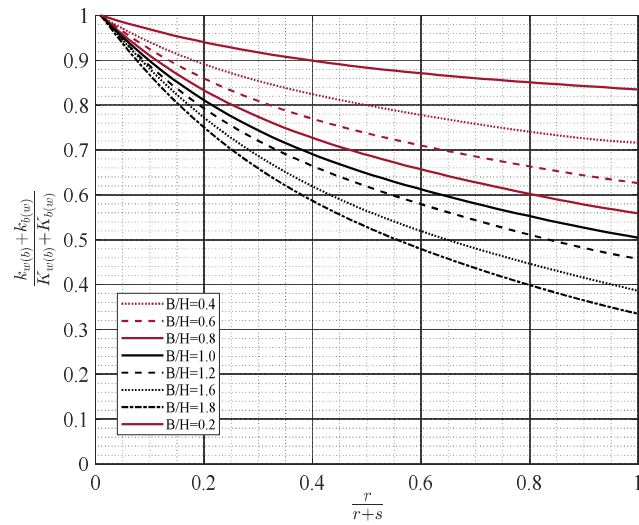


Figure 6. Control surface—control over stability contribution for elliptical sections [29].

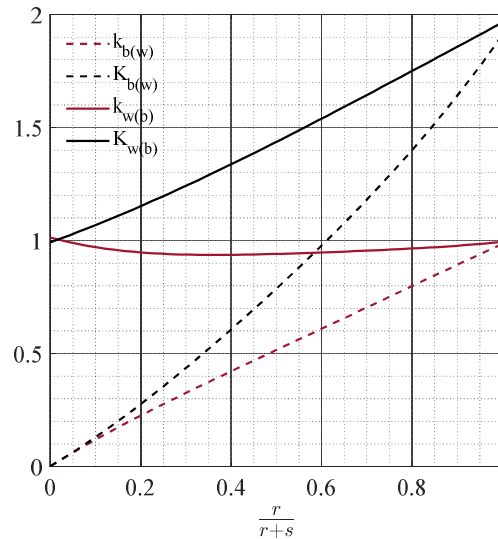


Figure 7. Control surface—interaction factors for fins on cylindrical bodies of circular section [29].

Propeller. The propeller model exploited four quadrant representation curves in terms of C_t and C_q given the standard design thrust K_t and torque K_q curves and the advance ratio $J = \frac{uA}{nD}$. An additional formulation for the lateral force $K_S = S/\rho n^2 D^4$ was included to encompass the unbalancing of tangential forces along the blade revolution in oblique flow. According to Harris [64] and Dubbioso [65], a linear coefficient including the crossflow velocity was obtained, counteracting the stern sidestep speed analogously in both the vertical and horizontal planes:

$$\frac{\partial K_S}{\partial v'} := K_{Sv} \tag{10}$$

$$K_{Sv} = 2.12J \left(K_Q - \frac{J}{2} \frac{dK_q}{dJ} \right)$$

This correction term is needed for very unstable submarines since it is the only term that is able to counteract the yaw/pitch motion when the stern control surfaces are aligned to the local inflow once the rotation has been triggered.

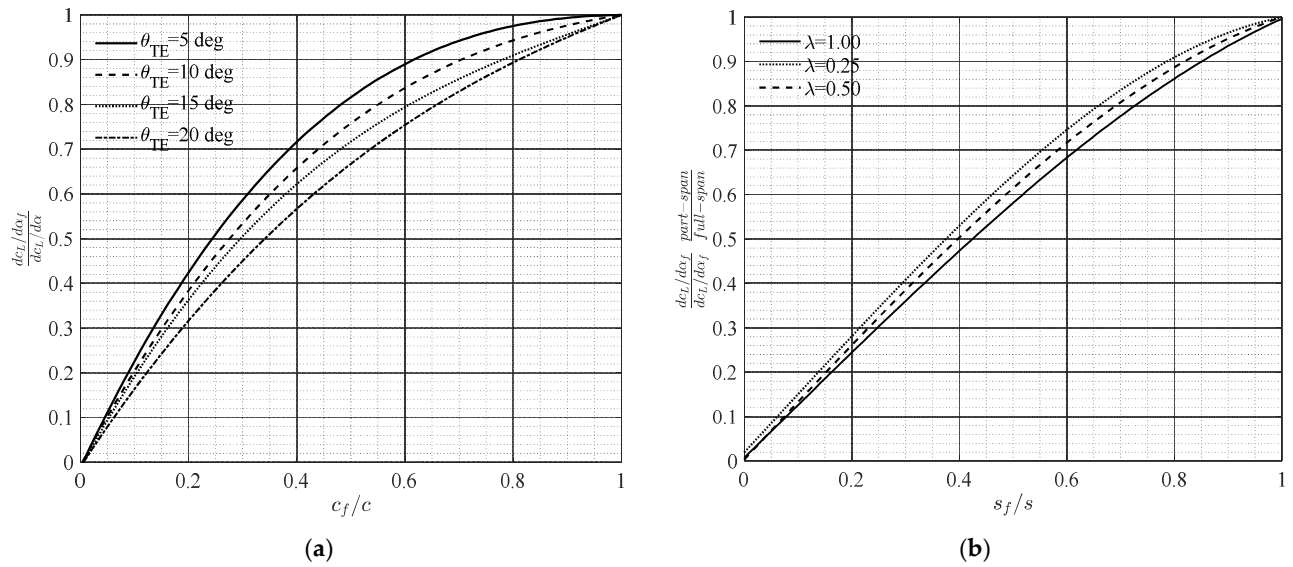
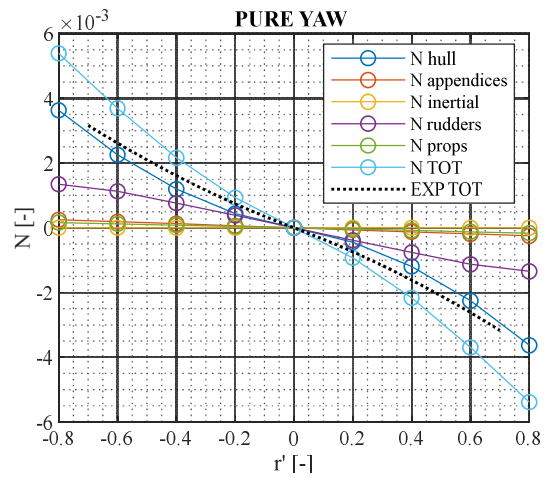
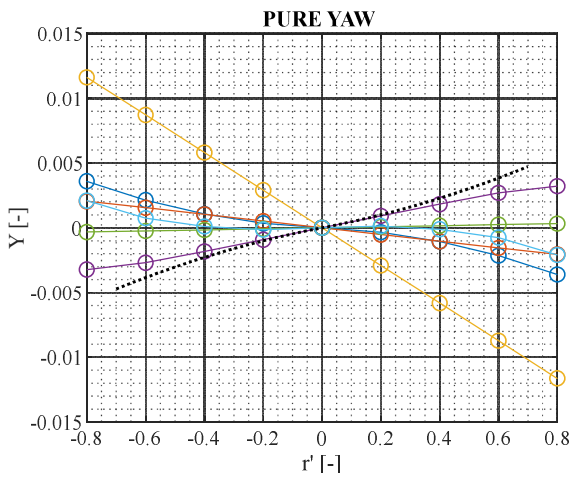
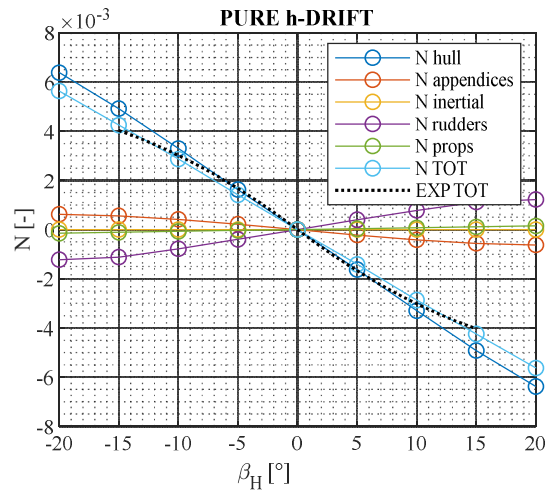
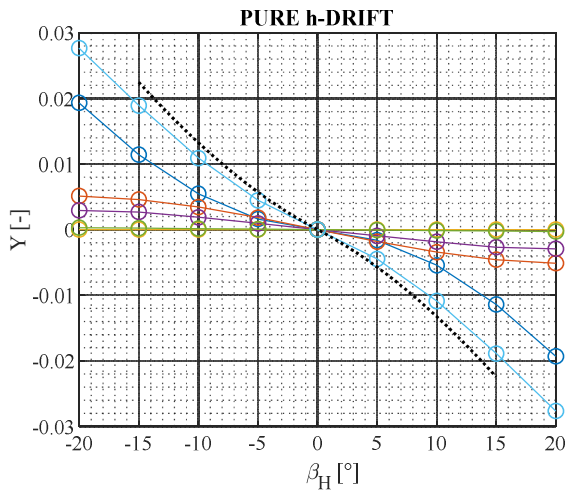
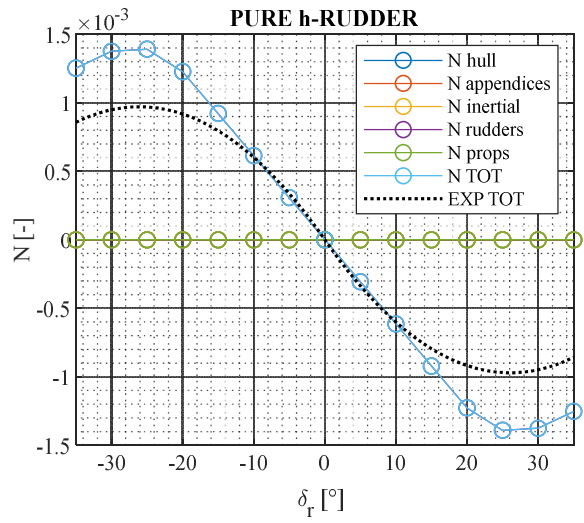
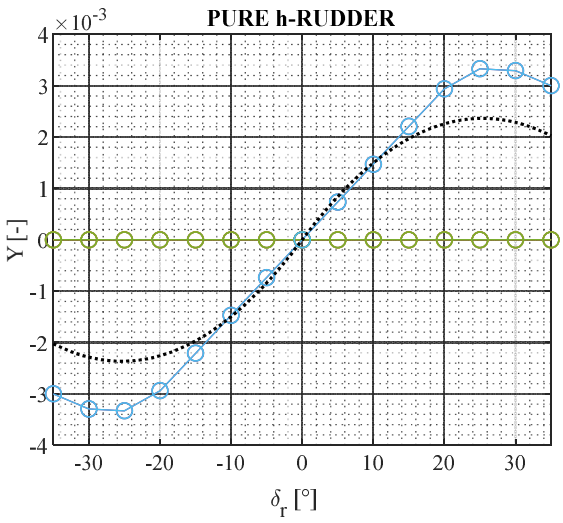


Figure 8. Flapped control surfaces—effect on lift [61]. (a) Chord-wise extent and trailing edge angle. (b) Span-wise extent and taper ratio.

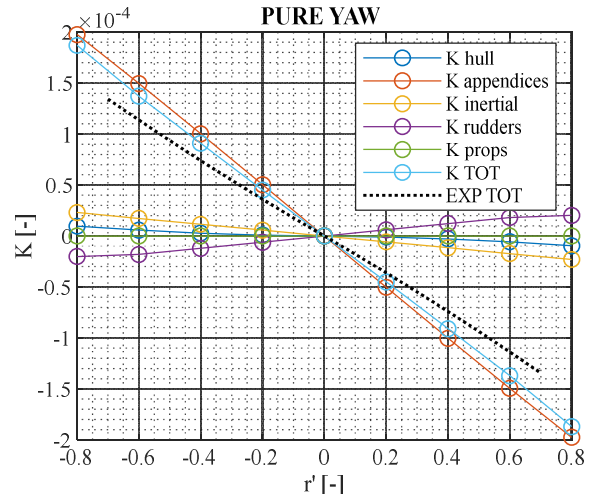
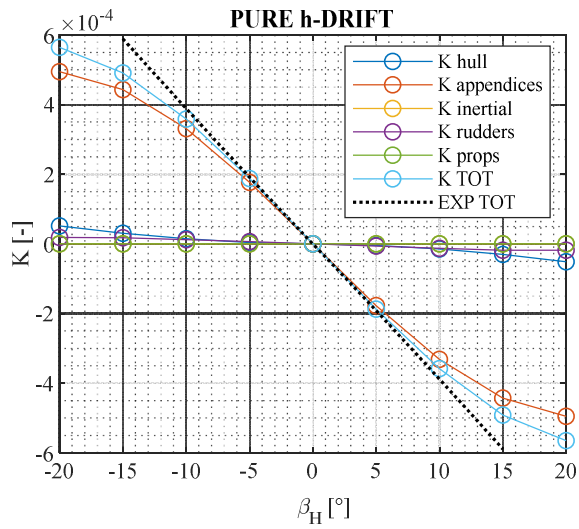
3.2. Captive Model Testing—Validation

Pure drift, pure yaw, and pure rudder tests on the horizontal plane as well as pure vertical drift (also called the angle of attack), pure pitch, and pure stern plane tests in the vertical plane were used to validate the captive model tests in a PMM approach with imposed kinematics. The corresponding lateral force Y , yaw moment N , and roll moment K were reported for the former series while the vertical force Z and the pitch moment M were studied for the latter series.

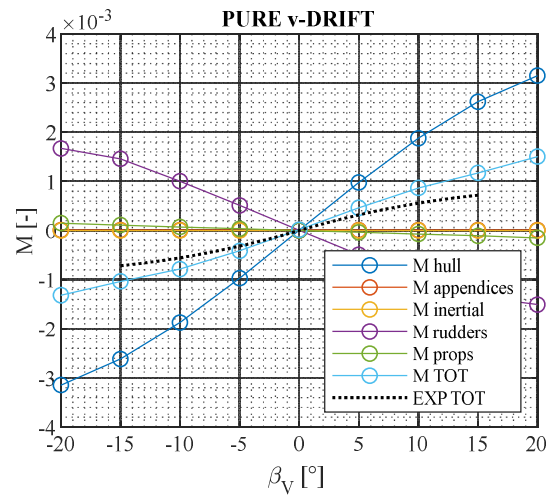
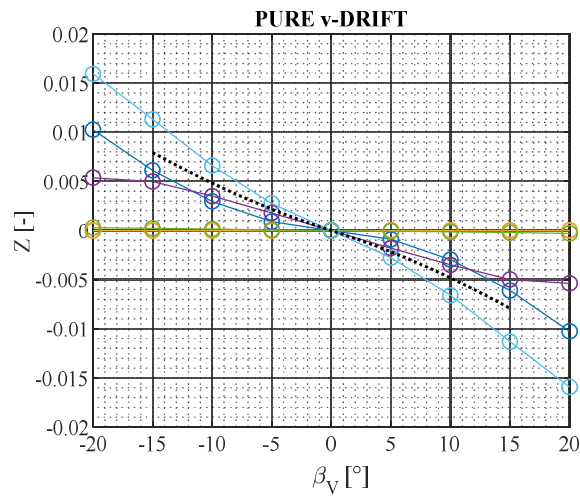
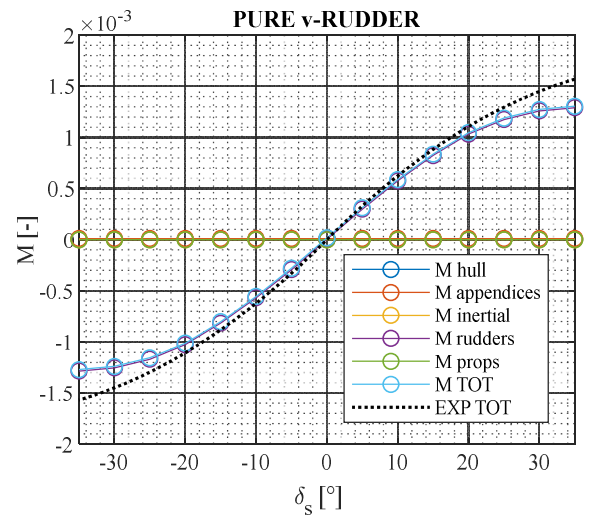
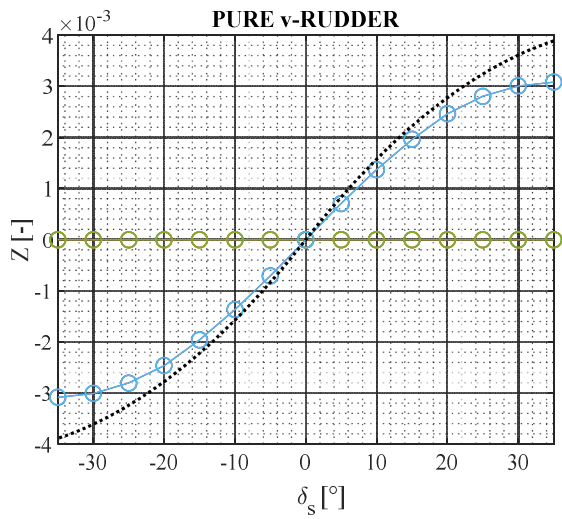
Results of the validation for the SMG, DARPA Suboff, and SWE vessels are shown in Figures 9–11, respectively, on the horizontal plane (a,b) and vertical plane (c). Numerical results are displayed by coloured solid curves (light blue for the totals) while the dotted black markers are used for the benchmark results. An overall good match with the experiments on both the manoeuvring planes is observed as well as a good agreement both in terms of linear and nonlinear trends. Moreover, the very good ability in splitting the contributions into the pure motions with fixed controls and plane executions is highlighted too. The best results in terms of matching experimental measurements are found for the SMG vessel, which is closer to modern submarine designs. Some discrepancies can be observed for the DARPA, which is the most unrealistic design, still preserving relevant accuracy.



(a)



(b)



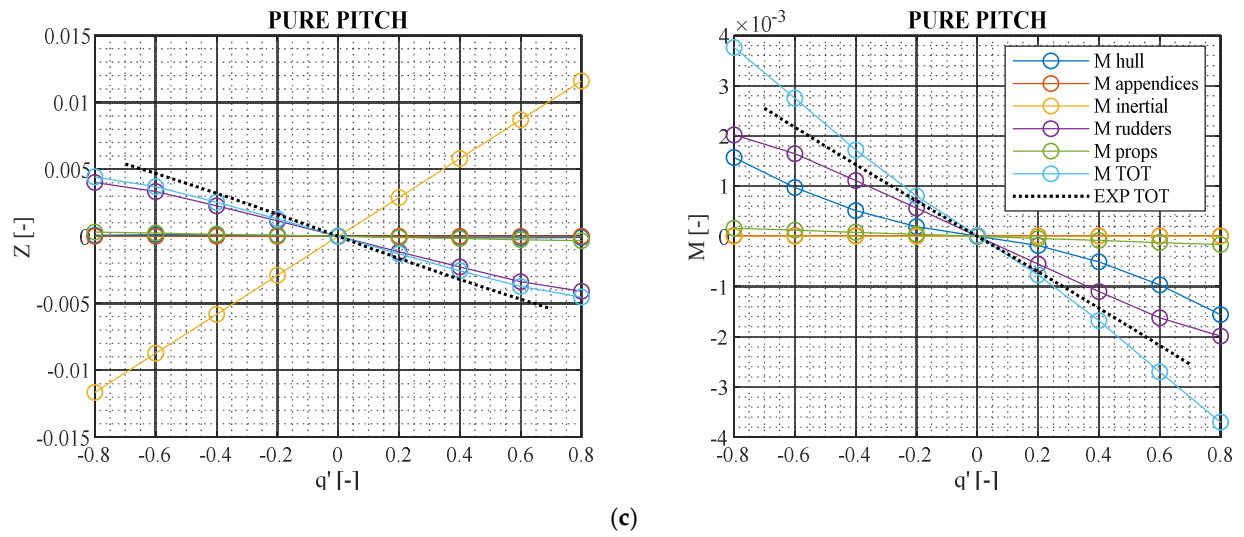
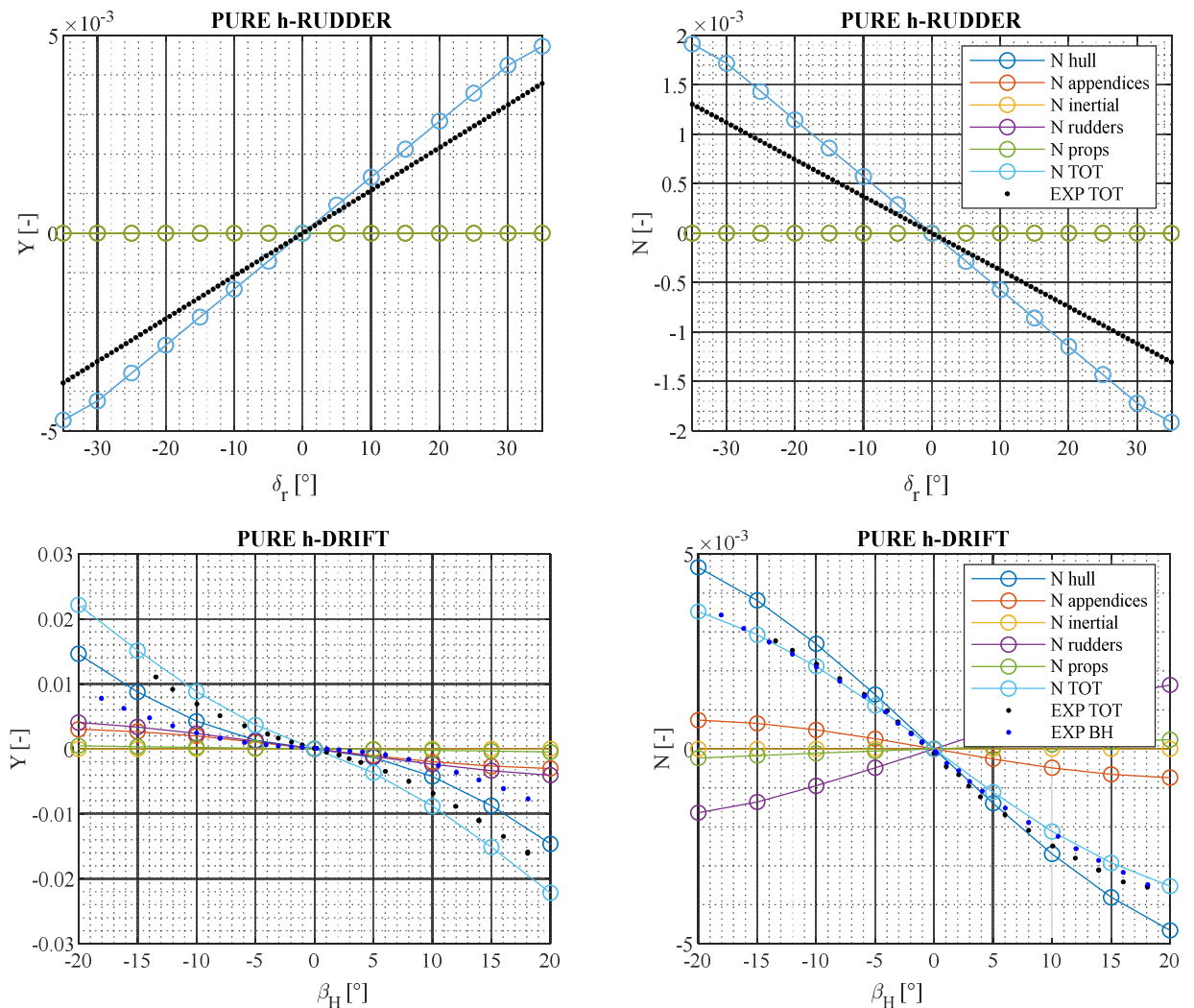
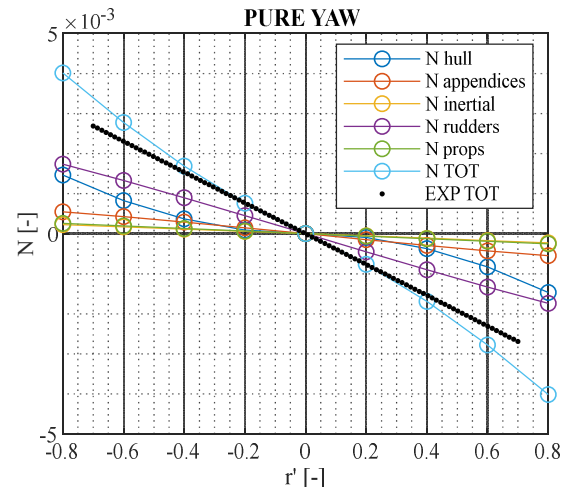
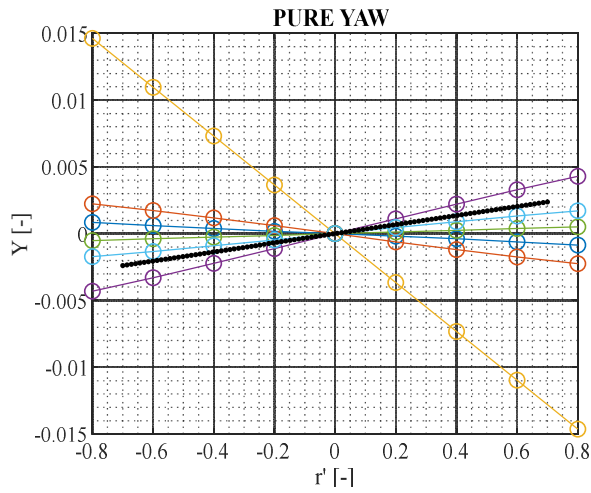
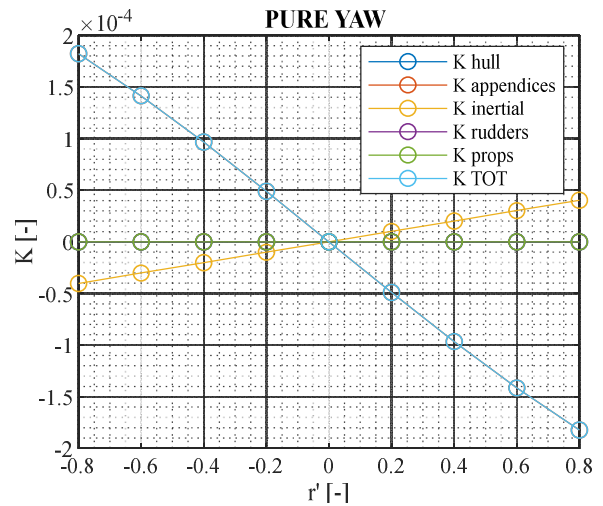
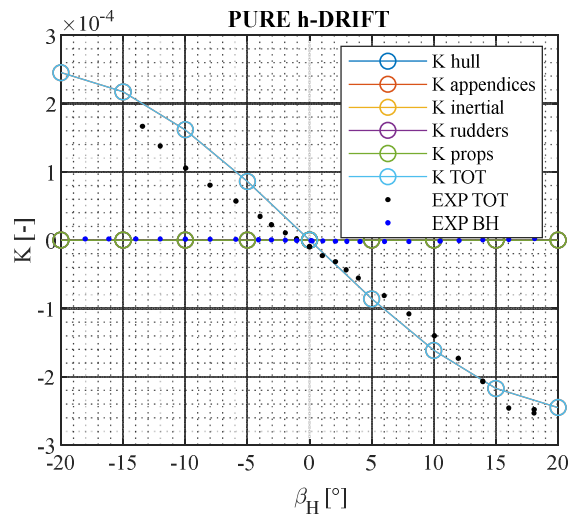


Figure 9. (a) SMG captive model testing validation—horizontal plane. (b) SMG captive model testing validation—horizontal plane roll. (c) SMG captive model testing validation—vertical plane.

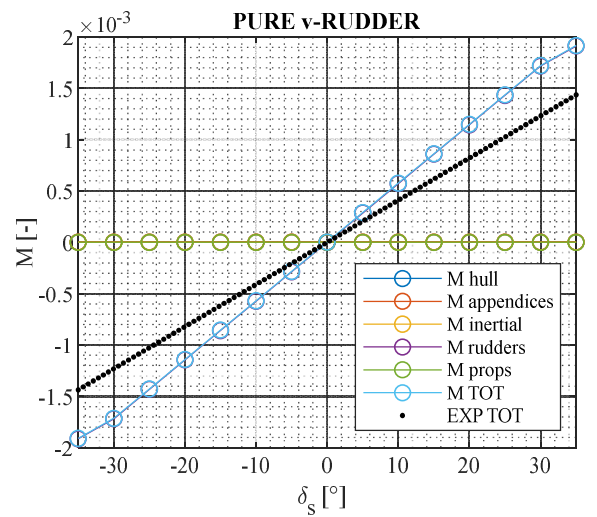
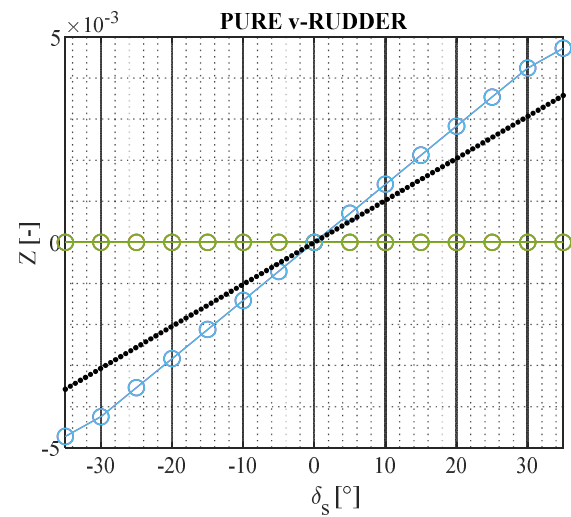




(a)



(b)



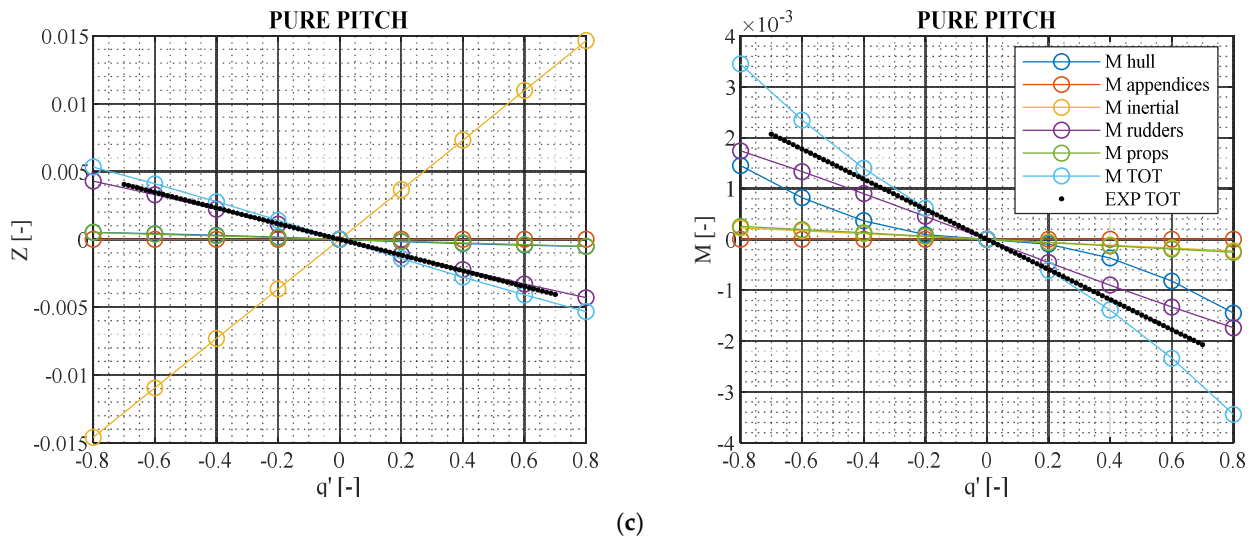
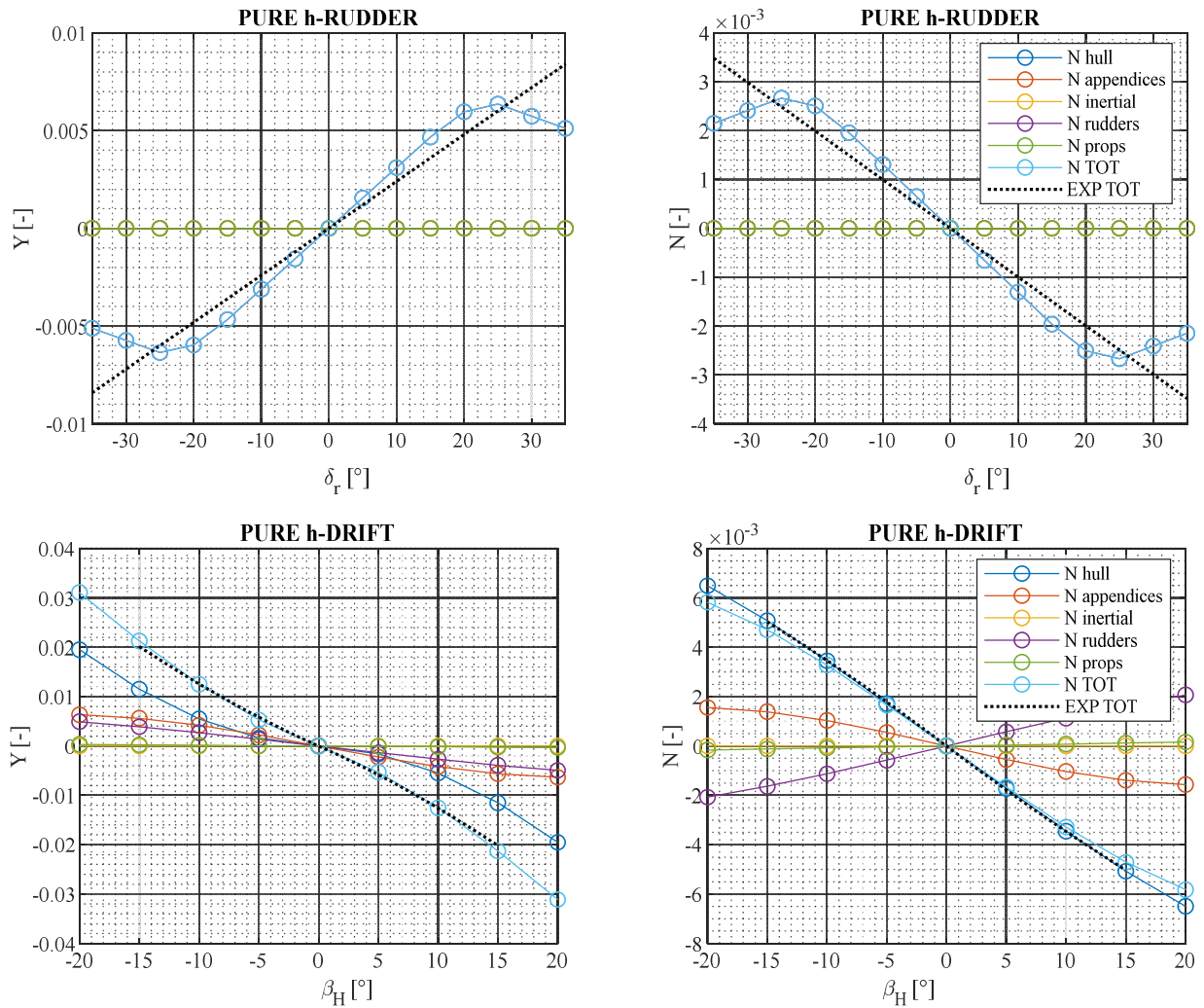
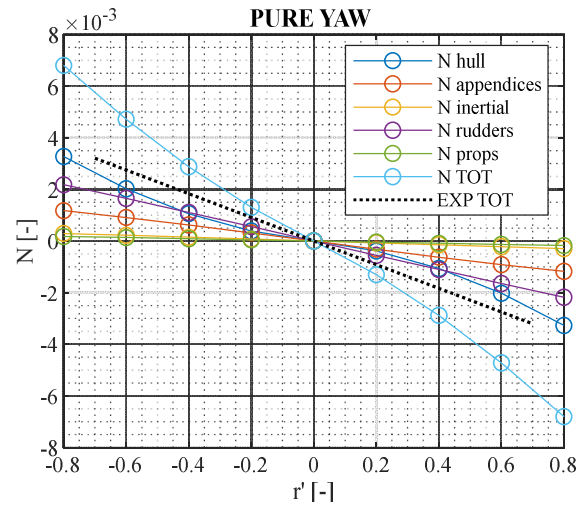
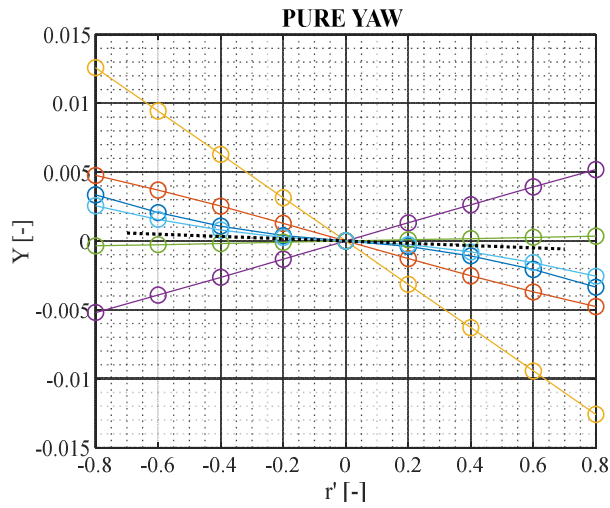
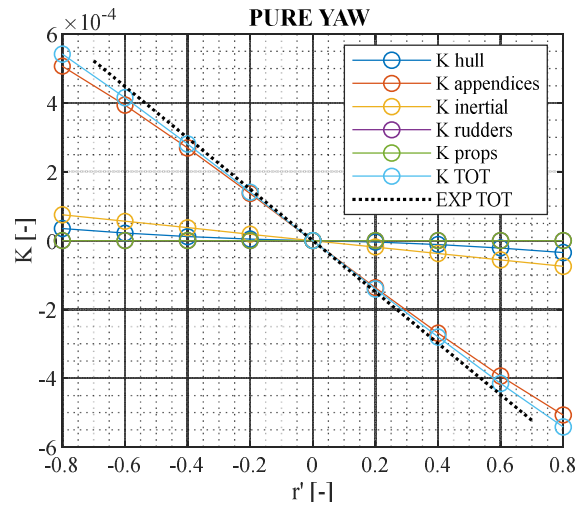
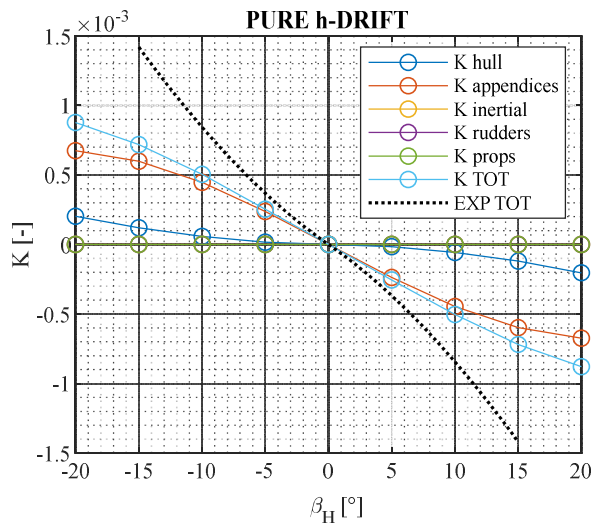


Figure 10. (a) DARPA captive model testing validation—horizontal plane. (b) DARPA captive model testing validation—horizontal plane roll. (c) DARPA captive model testing validation—vertical plane.

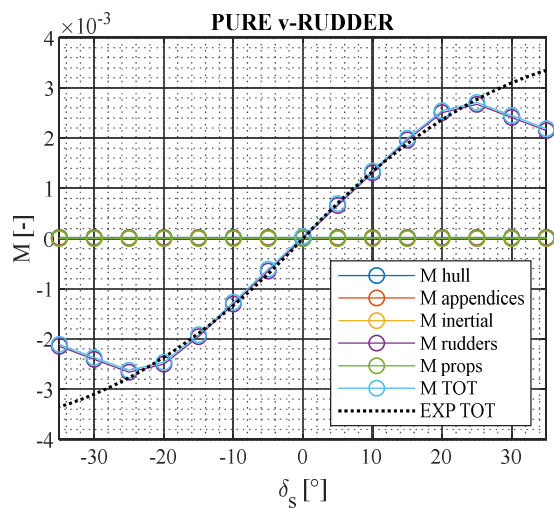
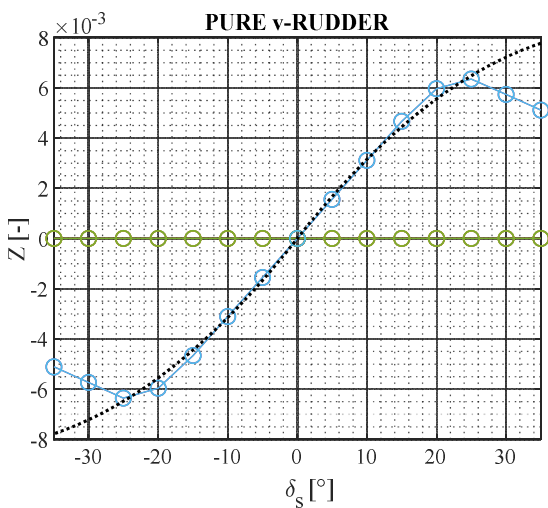




(a)



(b)



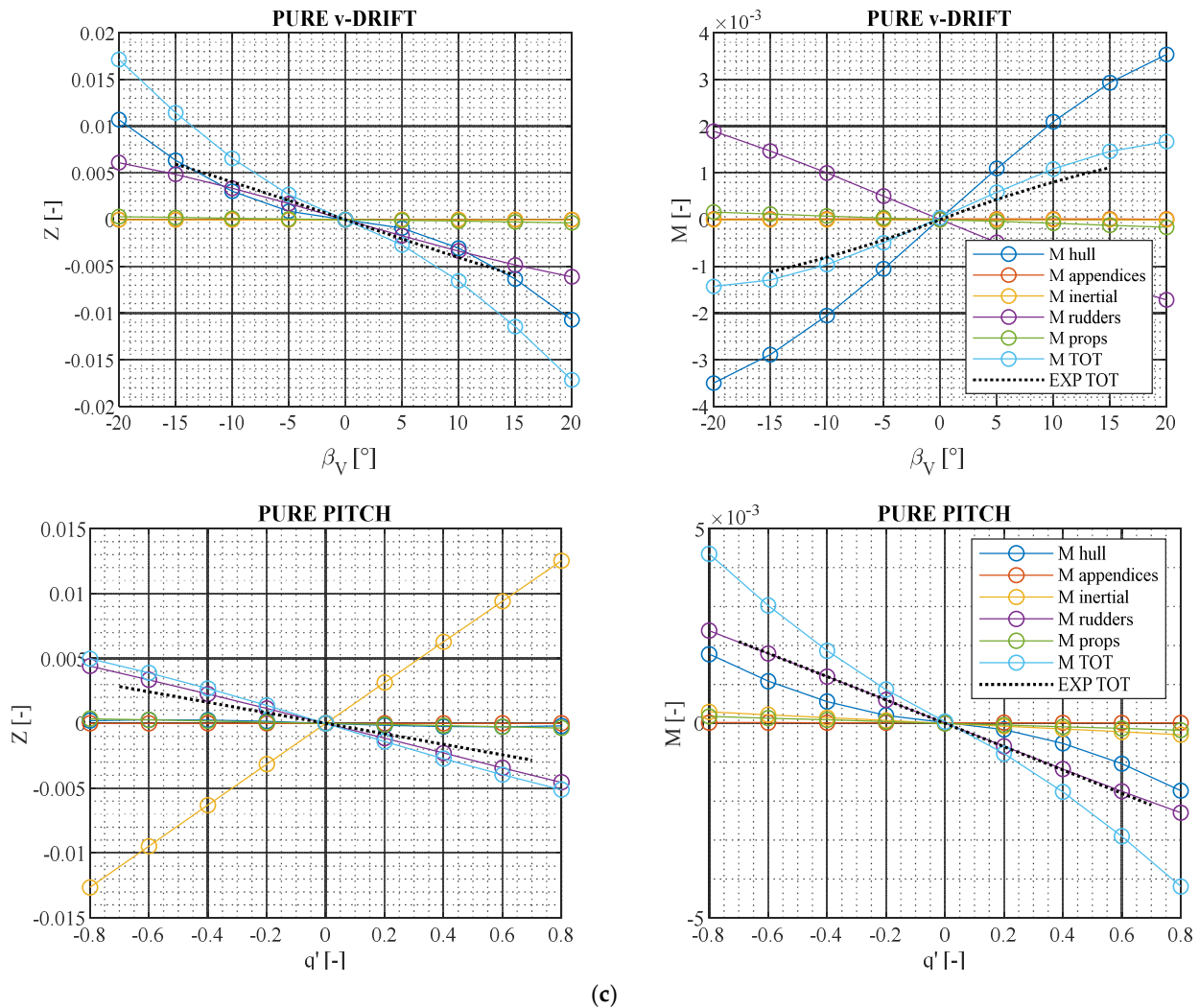


Figure 11. (a) SWE captive model testing validation—horizontal plane. (b) SWE captive model testing validation—horizontal plane roll. (c) SWE captive model testing validation—vertical plane.

3.3. Free-Running Tests—Validation

The dynamic simulation method was further validated by comparison against a model/full-scale free-running test. Classic turning circles and zigzag manoeuvres in the vertical and horizontal planes were considered. At this stage, each submarine was tested in its original design configuration.

The analysed manoeuvring parameters, shown in Figure 12, were the turning tactical diameters over the length (Dt/L) by varying the stern rudder angles (10–20–35°) and the zigzag overshooting sequence from the first to the third angle (#OVA) in the horizontal (10/10°) and vertical (5/5°) planes. The reference data are depicted with red markers while the simulated results are shown as the black solid line.

In the case of SMG, the experimental reference consists of both an experimental full-scale campaign (EXP FS) and a model scale simulation from an extensive captive model testing campaign (CMT MS). The SWE reference results come from mixed techniques [53] while the DARPA Suboff belongs to two different simulated datasets, revealing a huge dispersion due to the highly unstable design of this vessel [51,52]. Indeed, small variations in the stability index near to zero led to the relevant spread of the results.

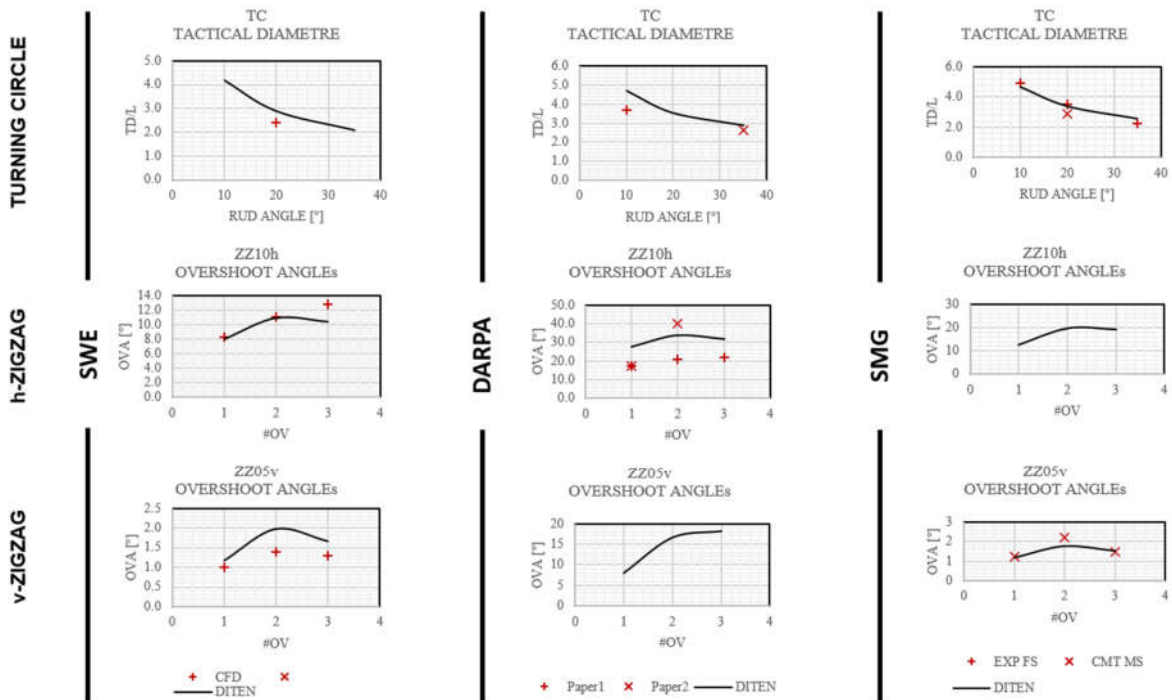


Figure 12. Manoeuvring validation.

Overall, the agreement is satisfactory. The best match is, again, found for the SMG design. Nevertheless, results for the DARPA Suboff test case should be considered satisfactory too: To compensate for the linear instability, the vehicle relies on strong nonlinear effects that are particularly challenging to be properly modelled and measured.

It is worth noticing that one of the valuable features of the proposed approach is the capability to treat arbitrary geometries and variable stability thresholds, dealing with results that might change significantly among various configurations. In terms of manoeuvrability performance, errors up to 0.3L in turning and 2.5° of overshoot (in the horizontal manoeuvre) are generally considered satisfactory in the reference literature.

4. Manoeuvring Results

A detailed analysis of the manoeuvring performance of the SMG vessel in both intact and degraded operating conditions was carried out. This study focuses on the comparison of the performance in both conditions with particular attention to a speed-dependency analysis. Moreover, the two possible stern plane configurations, i.e., x- and +-planes, respectively, were compared, providing a detailed design matrix that might ideally support the decision-making process at an early stage.

4.1. Design Matrix

The analysis carried out on the baseline SMG design (original) systematically accounts for variations of the following quantities:

- The sizing and position of all the appendages (a sail) and control means (movable percentage and +- vs. x-configuration);
- The weight and stability properties (longitudinal centring and restoring BG);
- The sectional and global slenderness of the bare hull (midship sectional area A_x , dimensional ratios L/B and H/B , and displacement);

The analysed parameters have been varied out of typical ranges to better highlight the sensitivity trends with respect to the manoeuvring performance.

For simplicity, the only variations in the resisting diameter, i.e., the breadth B , were endorsed by varying the volume of the vessel, i.e., the displacing resistant hull; the remaining volumes within the deck, keel, and sail, which form the hydrodynamic hull, were considered neutral. According to this, the following notation has been used to distinguish the hydrodynamic and manoeuvring effect, even if the modification is virtual and not compliant to any design criteria: “ ∇ ” means a transformation at a constant volume while “ $*$ ” refers to fictitious transformations without preserving volume. While scaling the hull, all the appendages and control surfaces were kept constant by only shifting the mounting locations consistently.

The following variations were considered:

- *Hull $-10\% Ax^{\nabla}$* —hull reduction of -5% in height H and breadth B (i.e., -10% transverse section Ax), same volume; that is about $+10\%$ length.
- *Hull $+10\% H/B^*$* —fictitious increment of hull aspect ratio ($+5\% H$ e $-5\% B$).
- *Hull $+10\% H/B^{\nabla}$* —from the previous $+10\%L$ to compensate for the volume loss.
- *Hull $_H = B Ax^*$* —modification of the transverse section to axial symmetric, i.e., $H = B$ maintaining the transverse section area Ax constant. This results in a $-10\% H$ e $+10\% B$. This fictitiously preserves the volume of the resisting hull without deck and keel.
- *Hull $H = B^{\nabla}$* —reduction of H to B , considering neutral the loss of volume from the deck.
- *Rud $+20\% s_0$* —increase of stern planes and rudders span about $+20\%$, i.e., $+20\%$ area.
- *Rud $+5\%L x_0$* —shifts ahead of stern planes and rudders about $+5\%L$.
- *Sail $+20\% s_0$* —raise of sail span $+20\%$, i.e., $+20\%$ area.
- *Sail $+20\% x_0$* —shift ahead of the sail 20% with respect to the original position (from $0.62L$ to $0.75L$).
- *LCG and $B +10\%L$* —virtual $+10\%L$ shift ahead of LCG e LCB. It does not include a shift of buoyant sections to compensate: the hydrodynamic hull is kept.
- *BG $+20\%$* —raise of $+20\%$ stability lever (lowering G).
- *Rud $2x$ rate*—doubling the steering slew rate.
- *Rud 80% Movable*—stern planes and rudders are all 80% movable (compared to the original configuration having 60% for the horizontal planes and 100% for the vertical surfaces).
- *Rud 100% Movable*—all stern planes and rudders 100% movable.
- *Rud “ $+Eq$ ”*—equal reallocation of the total area of stern rudders and planes.
- *Rud “ $x-Eq$ ”*—rotation of the previous configuration to x -setup.
- *Rud “ $x-Eq$ ” $-20\% s_0$* —reduction of -20% span with respect to the previous.
- *Rud “ x ” $60\%m$* —reduction to 60% movable of the previous.

A comparison of the course stability indexes in the two planes, including the damping ratio at 50% of the full speed and the critical velocity (expressed in knots, full-scale), is reported. The initial validation of the latter is reported in Appendix B, providing a good agreement with respect to the experiments on both planes. In addition, results for the horizontal zigzag $20/20$ (ZZ20h) and the Meander test (MEs5b10) are shown. Both manoeuvres are described in detail in Appendix A. The results are summarized in Figure 13 for 10 knots full-scale vessel speed.

Original design. The original design realized tactical diameters between 4.6 – $2.5L$, respectively, with 10 – 35° rudder angles and dynamically responds to the ZZ10h with an overshoot in the range of 12.5 – 20° and ZZ05v in the range of 1.2 – 1.8° . The first value refers to the first overshoot while the second refers to an average measure in between the second and the third. The ZZ20h cannot be executed due to the stall of the planes, which does not benefit from the propeller wake acceleration or consequent stall delay. The MEs5b10 requested a second execution time of $1.4L$, leading to a maximum trim angle of 6.5° and a depth variation of $0.33L$. In terms of stability, the submarine was horizontally, marginally stable with $G_h = 0.06$ while on the vertical plane, $G_v = 0.67$ with a damping ratio $DR = 0.7$ at 10 kn and a critical velocity of about 3 kn.

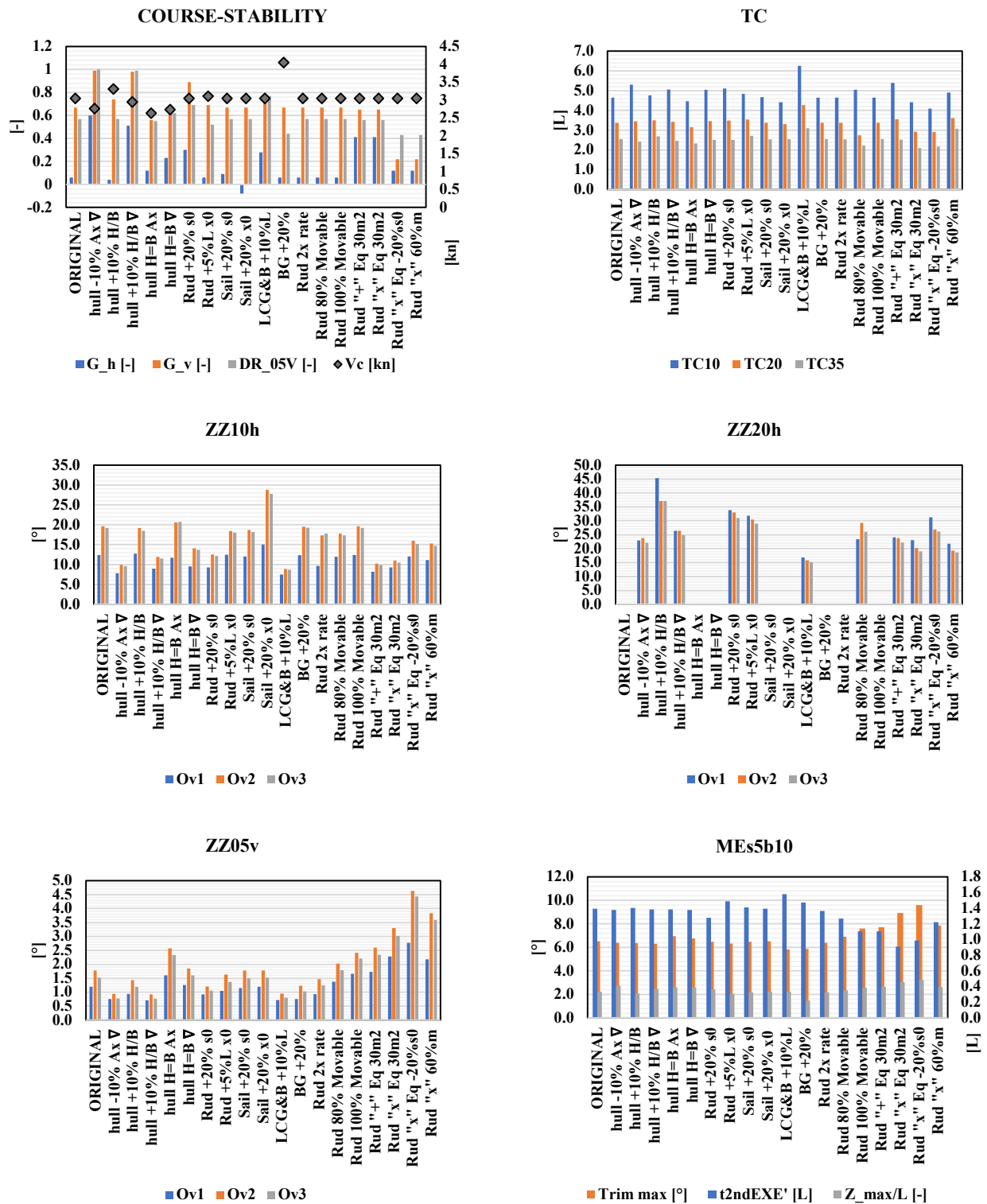


Figure 13. SMG—Manoeuvring design matrix—10 knots full-scale.

Hull -10% Ax ∇ . The transverse section reduction while increasing the length of the hull at the same volume increased the intrinsic stability of the vessel ($G_h = 0.6$, $G_v = 1$): The stern planes and rudders took advantage of the larger lever arm while the hull sizing

reduced with respect to the control surfaces. Therefore, both the stability coefficients increased. This benefitted the manoeuvres, halving the overshoots (about 10° -h 0.75° -v) at the cost of widening the turning diameters for small helm angles. For larger angles, the obtained nondimensional turning diameters were comparable. The circles, in terms of absolute dimensions, would all be larger due to the increased length. The increased stability allowed for the execution of the ZZ20h with overshoots angles of about 22.5° -h on average.

Hull +10% H/B*. The hull aspect ratio increase did not have any relevant effect on the manoeuvring performance. On the vertical plane, the reduction of hull projected area with respect to the stern planes slightly reduced the overshooting. On the other hand, the horizontal plane manoeuvre remained the same. The only exception was the feasibility of the ZZ20h, notwithstanding the large overshooting angles (about 40° on average). When the variation of volume was compensated by increasing the length, **Hull +10% H/B ∇** , there was a benefit in stability, as in the previous case.

Hull $_H$ = B Ax*. The axial-symmetric design of the hull keeping the sectional area A_x opposed the stability on the vertical plane due to the diameter increase, which resulted in more relevant hull hydrodynamic forces compared to the control term. The overshoot raised on average to about 2.5° -v. On the horizontal plane, the manoeuvres were almost unaltered. Vice versa, the solution **Hull $_H$ = B ∇** , for which only the neutrally buoyant volume within the deck and keel was eliminated by keeping B constant, experienced some advantages exactly in terms of the horizontal plane stability (G_h raises to 0.23). This reduced the horizontal overshoots to about 15° (-25%), widening the circles about $+0.5L$ for small helm angles but keeping the hard-over turning unchanged. The horizontal ZZ20h still remained unfeasible. The manoeuvres on the vertical plane remained unaltered.

Rud size and position. Increasing the stern plane size led to a significant improvement in the course stability on both planes ($G_h = 0.3$, $G_v = 0.89$). The horizontal and vertical overshoots diminished consequently (12° -h, 1° -v on average) due to the increased area and aspect ratio. The ZZ20h became feasible with overshoots of about 32° . The turning circles slightly increased for small execution angles, but the hard over settings identically reached a diameter of $2.5L$. Shifting ahead the stern plane mounting location slightly reduced the overshooting. The stability indexes remained unchanged at the cost of a smaller control and steering lever. The position of the control means played both in stability and controllability.

Sail. The sail sizing was not relevant in terms of manoeuvring since it is located around the pivot point during the turning and the neutral point (the pure drift centre of pressure). In fact, its angle of attack during the manoeuvre neutralized once the turning started. This avoided generating too huge of heeling moments. In this case, the sail was positioned at $0.62L$, astern the neutral point, which was located at about $0.82L$. The stability index in the horizontal plane slightly raised ($G_h = 0.09$) with minor reductions of the overshooting (-2° -h). Its specific positioning pulled back the neutral point around $0.75L$ while increasing the resistance to yaw. Vice versa, pushing the sail ahead to $0.75L$ had a destabilizing effect, causing a relevant increase of the overshoots (up to 28° -h during the ZZ10h). Correct longitudinal positioning is then a key feature of the design. Moreover, the smaller the angle of attack on the sail and/or the smaller the vertical extension, the smaller the snap-roll. The effects in terms of turning the circle are less relevant except for the heeling.

Slew Rate. The increase of the slew rate to 200% was ineffective in all the transients. All the overshoots diminished irrelevantly. The vehicle experienced a fast reaction, thus was not sensitive to this variation.

Mass. The virtual shift ahead of the centre of mass intrinsically increased the stability index of the vehicle. The centrifugal force that opposes to yaw moved ahead without modifying the hydrodynamics of the vehicle ($G_h = 0.28$, $G_v = 0.76$). However, this shift was fictitious and did not take into account any variation or shifting of the buoyant and

structural sections. In these terms, it is intuitive that a centre of mass positioned astern tends to make the stern drift outside the turn. On the contrary, the drift and yaw moments will tend to compensate and balance as the centre of mass moves closer to the neutral point. The benefits in terms of zigzag were significant ($<9^\circ\text{-h}$ e $<0.8^\circ\text{-v}$) but at the cost of slowing the vehicle reaction (second execution time 1.6L), i.e., the time constants. The ZZ20h could be realized with an overshoot of about 15° . On the other hand, the parameter was very sensitive in terms of turning, widening the tactical diameters around +1.6L with the smaller helm angle of 10° , and +0.6L with the hard-over setting. The variation of BG was not relevant on the horizontal plane except for the snap roll because of the larger lever arm between the lowered centre of mass and the vertical centre of pressure. The variation of BG was more sensitive in the vertical plane. The damping ratio reduced significantly (to 0.44) while the critical velocity increased up to 4 kn, which is a not desirable effect for low-speed manoeuvring. The increased restoring capability reduced the vertical overshoots to values smaller than 1.2°-v and slightly slowed down the dynamics. The response to the Meander test was slower and less stiff with maximum trim angles reduced to 6° and a depth change of 0.22L. The stern planes experienced more difficulty in counteracting BG to vary the vehicle angle of attack useful in changing depth. This was made clear by the increase up to 4kn of the critical velocity and the reduction of the damping ratio. The stability moment, indeed, became more influent with respect to the hydrodynamic control forces.

Rud movable area. The reduction of the movable portion of all the control surfaces to 80% (originally the rudders were at 100% while the stern planes were at 60%) led to a slight reduction of the ZZ10h overshoots while making it possible to realize the ZZ20h with overshoots smaller than 30° . De facto, the modification reduced the steering capabilities of the submarine, i.e., the only control action in the rudder and counter-rudder sequences. This triggered a dynamic system with the same stability properties (in stability terms, with a zero angle, 100% of the surface accounts in terms of stability—i.e., G_h does not vary). In terms of the vertical plane, the system response became faster and stiffer (since the original configuration considered a 60% movable area). By turning all the stern control surfaces to 100%, the vertical plane phenomenon increased, raising the overshoot to 2.5°-v , reducing the second execution time of the meander test (0.95L) and increasing the maximum pitch angle to 7.6° and the depth change (0.33L).

+Rud Eq. area reallocation. The fair reallocation of the area on the four stern control surfaces, all 100% movable, penalized the horizontal planes while improving the performance of the vertical ones (considering that the original design was unbalanced in terms of areas). The stability indexes changed accordingly [$G_h = 0.41$, $G_v = 0.65$]. Better controllability on the horizontal plane was experienced while the vertical manoeuvre became stiffer. The overshoots almost halved on the horizontal plane (around 10°-h on average) while doubling on the vertical plane (2.6°-v on average) with values almost identical to the solution, +100% movable, with the original distribution of areas. There was a relevant impact of the exciting and restoring forces in this comparison. On the other hand, the ZZ20h became feasible with a maximum overshooting angle of about 25° .

x-Rud Eq. setup. The variation from the equivalent +-setup to the equivalent x-setup increased the control action by about an ideal factor $\sqrt{2}$, i.e., +40%, keeping the stability indexes constant. It resulted in $G_h = 0.41$ and $G_v = 0.65$, maintaining the same area as that of the +-setup. In terms of manoeuvrability, this narrowed the turning circles. The horizontal overshoots remained unchanged. The ZZ10h overshoots rose to a negligible quantity due to the higher exciting forces while they were slightly reduced in the ZZ20h to 23° . On the vertical plane, the overshooting stiffened at about 3.3° : The configuration almost doubled the overshooting if compared to the original design. This is particularly evident in the Meander test, making this setup the most responsive. The second execution time halved (0.9L), generating a higher trim angle (9°) and larger variations of depth (0.45L) due to the higher hull-induced angles of attack. This means that smaller stern plane

angles may be sufficient to reproduce the same manoeuvring abilities of the original design due to the higher pitching effectiveness.

x-Rud Eq. variations. Considering the above x-setup reallocation, the reduction of the span to the extent of -20% destabilized both the manoeuvring planes again, changing both the overshooting to 15° -h and 4.5° -v. The vertical plane then became less dampened. The reduction of the movable surface to 60% (coupled with the above span reduction) slightly reduced the vertical overshooting by reducing the exiting triggering control force but still with a substantial difference from the original design. On the other hand, the horizontal plane manoeuvring was not particularly modified but experienced a reduction of the turning ability.

In conclusion, the capability of restoring exactly the +setup manoeuvring features cannot be achieved directly with an x-setup unless segregated control on the two manoeuvring planes is undertaken. The +setup indeed benefits from an intrinsically segregated stability and controllability featuring the two manoeuvring planes. On the other hand, the x-setup is more effective in terms of controllability, with analogous stability featuring, turning the same control planes to be more effective. Moreover, the latter setup offers a convenient redundancy of allocation on the two manoeuvring planes. The x-setup control action can be suitably tuned by reducing the allocation angles according to the manoeuvring plane to best meet the desired execution readiness and stiffness.

In terms of design features, the x-setup presents fewer limitations in terms of mounting given the fact that the lower keel line does not limit the extension of the planes directly in the vertical direction, such as it does for the lower rudder of the +setup. In terms of operability, the solution is also effective in case of failure, such as a jammed or lost control surface, as will be demonstrated in the next sections.

4.2. Speed-Dependency

The speed dependency analysis has been carried out by varying the velocity from 5 kn to 25 knots at full scale. The extreme value of 25 kn has been included to extend the study to the highest possible operating speed and to provide trends over a broader range. Results for the +plane configuration and the equivalent x-plane configuration are shown in Figures 14 and 15, respectively, focusing on the attitude angles reached by the corresponding submarine. Dive Fail test "DF" manoeuvre is included (the 'DFs5b10n7_15s60s') according to the definition described in Appendix A.

The speed effect was relevant in terms of overshooting and dynamic attitude during the transient phases of all the zigzag and the Meander tests. This is due to the balance between the inertial and the hydrodynamic forces on the horizontal plane and the restoring forces on the vertical plane. By increasing the speed, the overshoot angles doubled in both planes. Both the attitude and depth changes increased accordingly. Vice versa, no effects were expected in terms of turning apart from travelling the same turning circle with a different velocity and different heel angle.

By dropping the speed, the vertical controllability of the +plane configuration decreased. Reaching the 5° trim threshold angle with a helm execution of 5° then became impossible. The control action was not sufficient to create the pitching moment if compared to the restoring capability. Indeed, the lower the velocity, the lower the hydrodynamic drift moment on the hull collaborating with the plane's action. The plane's moment became irrelevant and cancelled out with the hull forces. By excessively increasing the speed, over-critical trim angles greater than 20° may be reached both in terms of the Meander test and dive-fail crash-stop. In the latter manoeuvre, the head achieved 11L with a depth change of 5L, reaching unfeasible trim angles.

On the other hand, the x-setup was more sensitive overall to the stern-plane actuations, spanning over greater ranges of overshoot angles by changing the velocity. This configuration maintained controllability at the lower velocity too, turning feasible both the vertical zigzag and the Meander test. Finally, it is evident that excluding only one

of the stern planes led to a relevant lateral reach in the dive fail-stopping mode but significantly diminished the longitudinal reach to a maximum of 6.5L.

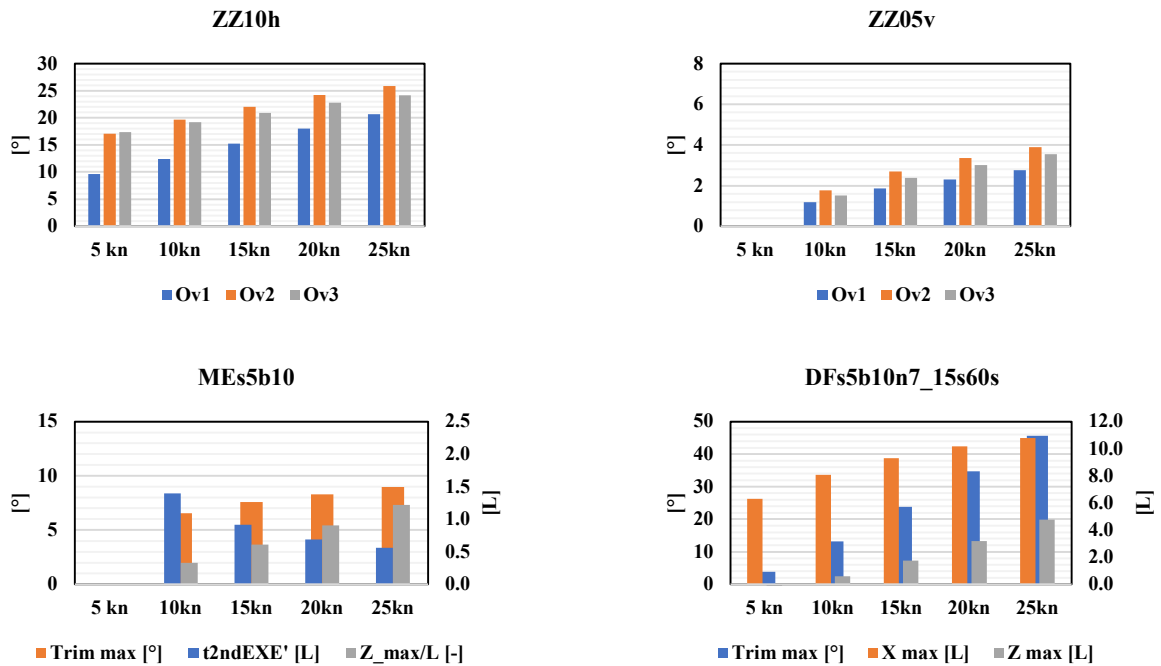


Figure 14. SMG +-Eq—Manoeuvring speed dependency.

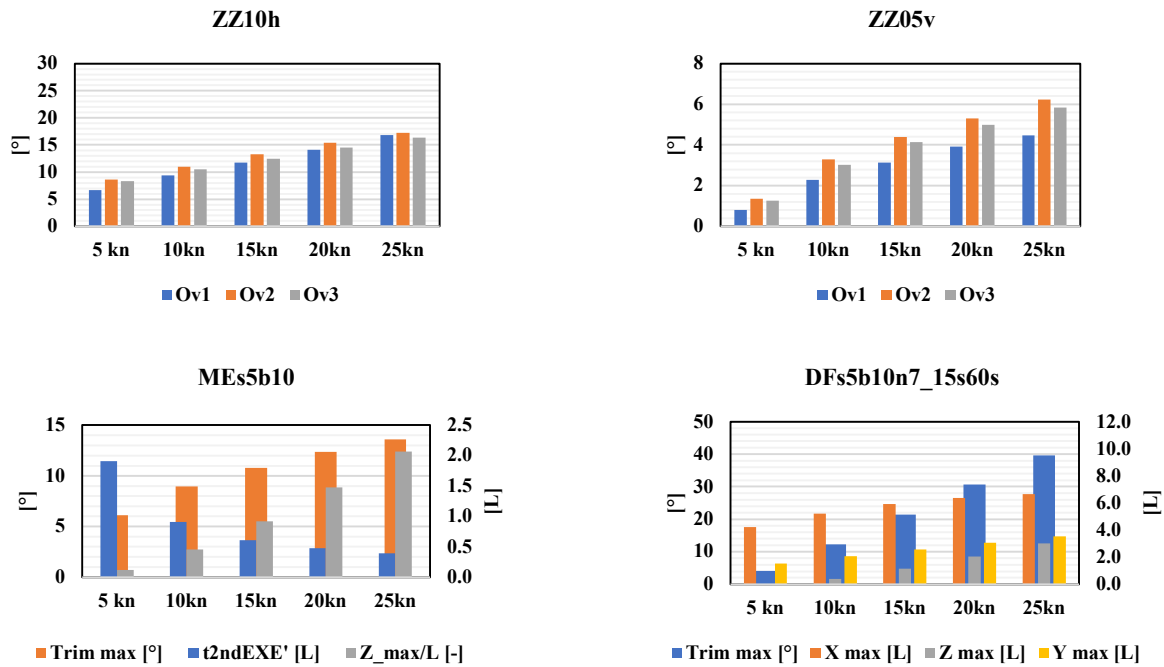


Figure 15. SMG x-Eq—Manoeuvring speed dependency.

4.3. Failure Scenario

The failure of the stern steering planes was modelled by considering the surfaces to be jammed in a sequence at defined angles or that they would be lost. According to Figure 16, in the case of horizontal manoeuvre with +setup, the failed plane was the lower vertical (#1) while for the x-setup it was the portside lower (#1). In the case of vertical manoeuvres with the +setup, the failed plane became the portside horizontal (#2) while it remained the same (#1) for the x-setup. Indeed, with the x-setup, it was not possible to segregate the degrees of freedom in terms of failure since it was redundant in terms of controllability in the crossed planes. It was also assumed that in the +-configuration, the opposing rudders, and planes could be executed decoupled, which is not the case with some existing submarines. If this assumption could not be met, the handling of the vehicle would be completely lost without any chance to manoeuvre further.

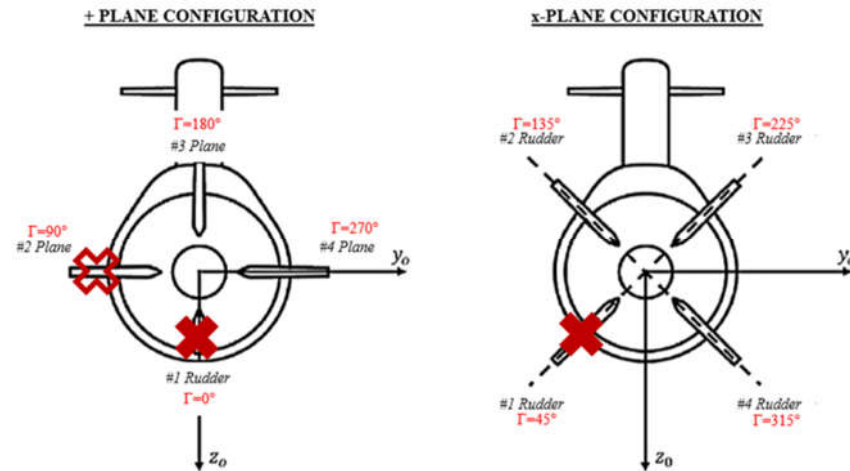


Figure 16. Stern-plane failures.

The control surfaces were jammed respectively to 10–5–0° in the counter manoeuvring direction of the initial turning. They were alternated in favour or not in terms of overshooting. It was also considered the scenario with the complete loss of the control surface, i.e., not generating any force. The abbreviation used to identify each manoeuvre is 'xRFy', where 'x' is the rudder id, 'RF' stands for rudder failure, and 'y' is the jammed angle '10–5–0°' or the loss 'L'. All the manoeuvres were approached at 10 kn.

Figure 17 displays the turning circle results while Figure 18 shows the horizontal zigzag comparison. As a visual support, the trajectory plots only depict the turning circles (35° and 10°) and the horizontal zigzag (10/10°) in the intact and 1RF5 condition—i.e., plane #1 failure at 5°. The histograms, on the other hand, report the whole series of jammed and lost rudders in terms of tactical diameter and overshooting sequences. The complete set of results, including the heel and trim of the submarine, are shown in Appendix C—Figures A7 and A8.

A smaller loss of turning ability but with relevant dynamic longitudinal and transverse attitudes was experienced by the x-configuration compared to the + configuration, as shown in Figure 17a,b, respectively. Indeed, the unbalancing of the whole set of the four control surfaces had a stronger effect in terms of roll and pitch moment if no countermeasures were adopted. The turning ability reduction was evident in the TC10 but was progressively lost while rising the helm angle to the TC20 and TC35, leading to turning diameters like the original ones. This is due to the stall of the jammed control surface which was set to a geometric counter-manoevring angle, i.e., an effective counter-angle magnified by the drift. An overall destabilization was observed if the control surface was lost, narrowing the circles whichever the helm angle. Finally, in the x-setup, the attitude variation led to modifications of the vehicle angle of attack, and, in turn, to

relevant depth-changing velocities. These should be compensated by using the bow planes or by setting differential angles around the average stern plane’s setpoint. For instance, the latter differential correction on the stern planes of 5° and 10° with a time delay to the execution in the trajectories is proposed. This means that, e.g., from the turning setpoint, the portside and starboard side planes set asymmetric to pitch the bow down, i.e., to $35^\circ \pm 5^\circ$ and $35^\circ \pm 10^\circ$, while keeping the turning contributions. As a result, the emersion velocity is nullified with a minor turning ability decay. The +-setup experienced wider turning diameters, especially for the smaller helm angles, but then exhibited narrower circles at the higher angles.

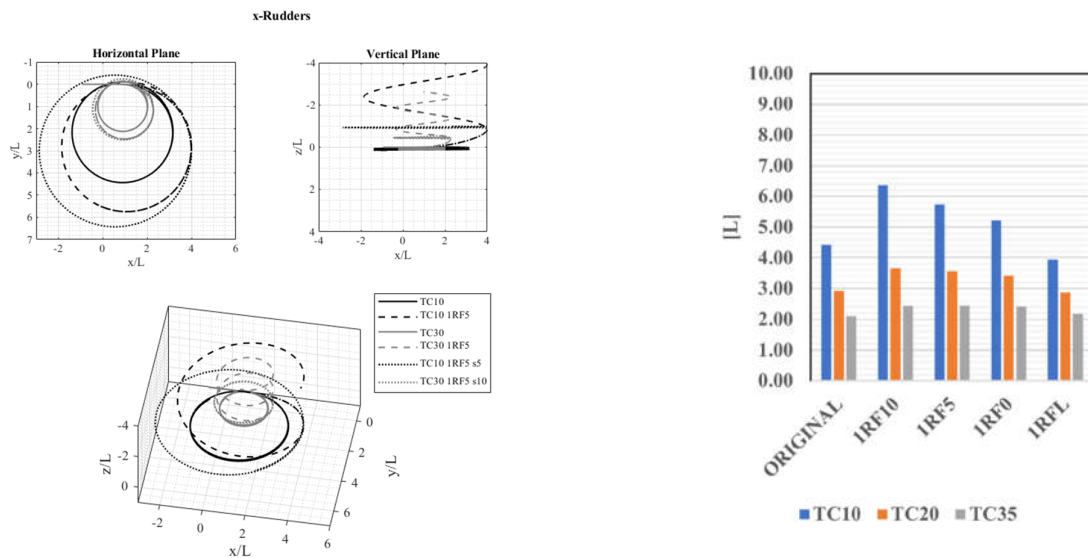
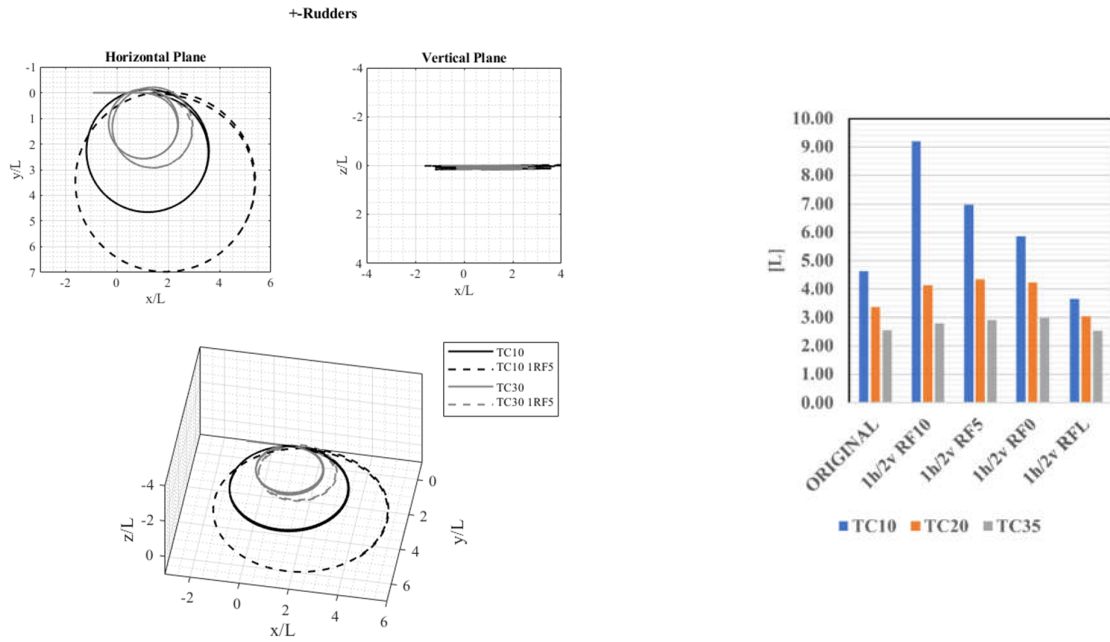


Figure 17. (a) SMG +-Eq—Turning circles in #1 plane jammed or lost condition. (b) SMG x-Eq—Turning circles in #1 plane jammed or lost condition.

As shown in Figure 18a, the zigzag stability and controllability features were strongly degraded in the +-configuration. Given the residual controllability of only one control surface, there is no safety margin when the jammed angle is large or if the surface is lost. In fact, the manoeuvre cannot be realized when the surface is lost or if jammed at 10°. The overshooting sequences reached 30° in the 1RF5 condition when not in favour of the turn direction. If the surface was jammed on the centreline, on the other hand, all the manoeuvres became stable, opposing the active trigger action of steering. Vice versa, as displayed in Figure 18b, with the x-setup, the residual effectiveness of the three control surfaces was still satisfactory in terms of yaw-checking ability also when the fourth surface was lost. All overshooting sequences were realizable and more than halved with respect to the +-setup. The benefits of the x-setup are evident in terms of readiness and control. The horizontal zigzag trajectories highlighted the loss of symmetry starboard to the portside, inducing the vehicle to drift progressively to the portside. Moreover, the x-setup did not suffer a relevant loss of the control period in the degraded condition compared to the intact condition. The +-setup reduced the control readiness and led to larger flaws in terms of yaw-checking, increasing the overshoot angles. In case a straight path needs to be recovered, the x-setup allowed for a more flexible redundancy in differential setpoints to achieve this goal.

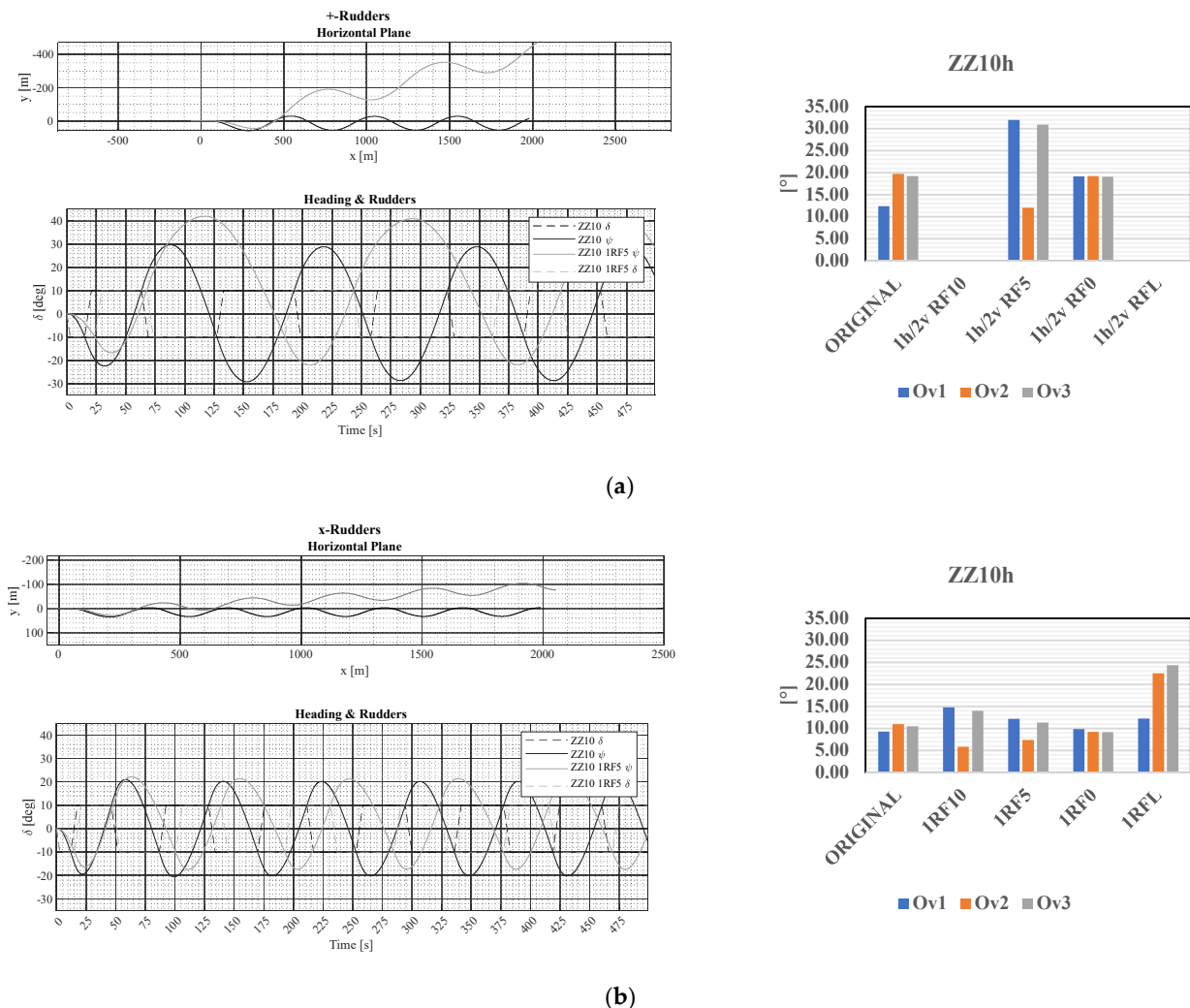


Figure 18. (a) SMG +-Eq—Horizontal zigzag in #1 plane jammed or lost condition. (b) SMG x-Eq—Horizontal zigzag in #1 plane jammed or lost condition.

5. Conclusions

A thorough, modular modelling approach to simulate submarine manoeuvring has been developed and validated in six degrees of freedom both on the horizontal and vertical planes. The ability to capture the heterogeneity of a fleet of three very different submarines in terms of design and manoeuvring implications, ranging from the highly unstable DARPA Suboff to the most realistic SWE and SMG, has been proven by the comparison of the numerical results against experimental, available data. The validation process has confirmed the reliability of the proposed method with respect to both captive model testing and free-running manoeuvres.

The method has then been applied to study the intact and degraded performance of a realistic submarine in different operating scenarios, proving its effectiveness as a reliable design tool to be used at an early stage of the design process. The effect of all the main geometrical parameters with the details of the hull, sail, and control surfaces has been studied as well as the speed-dependent handiness of the vessels, which is of relevant concern for the controllability in both planes. From the comparative analysis carried out on the stern plane configurations, the x-setup positively demonstrates valuable features in terms of controllability ranging from the lowest velocities on both the manoeuvring planes at the cost of stiffer executions in the vertical response. The greater effectiveness in triggering the manoeuvres leads to the conclusion that smaller execution angles may be selected. This relieves a greater safety margin in terms of manoeuvring given the evidence, and also, in case of jammed or lost surface, such a setup guarantees satisfactory, even if degraded, handling features, but only if the vehicle attitude and depth are monitored and kept under control by an automatic or manual system.

Author Contributions: Conceptualization and methodology, B.P., G.V., G.M. and M.V.; software and validation, B.P. and G.V.; formal analysis and investigation, B.P.; resources, M.V. and M.F.; data curation, B.P.; writing—original draft preparation, B.P.; writing—review and editing, M.V. and G.V.; visualization, B.P.; supervision, M.V.; project administration, M.V. and M.F.; funding acquisition, M.V. and M.F. All authors have read and agreed to the published version of the manuscript.

Funding: This research received partial support from the Italian Ministry of Defence.

Acknowledgments The research activity described and discussed in this work has been in part developed during the ASAMS project (Aspetti Specialistici e Approccio Metodologico per la progettazione di Sottomarini di ultima generazione), financially supported by Italian Ministry of Defence, and in collaboration with Fincantieri.

Conflicts of Interest: The authors declare no conflict of interest.

Appendix A

Appendix A.1. Meander Test

The Meander tests is a pull-out manoeuvre from the vertical zigzag second execution. The test is apt to verify the vertical course stability of the vehicle after a disturbance, thus its ability to change depth and restore a constant depth course. It considers a combined action of the stern planes and bow planes to impress a maximized variation of angles of attack of the vehicle to change depth—see Figure A1: After the execution of the planes, when the vessel reaches a reference pitch angle, the planes reset to zero, and the stability in the vertical plane is verified. The test philosophy is analogous to a turning pull-out test to verify eventual residual velocities, in the present case, in terms of pitch oscillation damping and diving velocity. The presented parameters refer to the second execution time in terms of promptness, and the maximum overshoot trim in attitude and depth change to verify the depth change capability and the stability in case of oscillations. The manoeuvre, called “MEs5b10”, stands for the execution of the stern planes at 5° “s” and the bow planes at 10° “b” to pitch down. The characteristic quantities are reported in the table and timeseries of Figure A2.

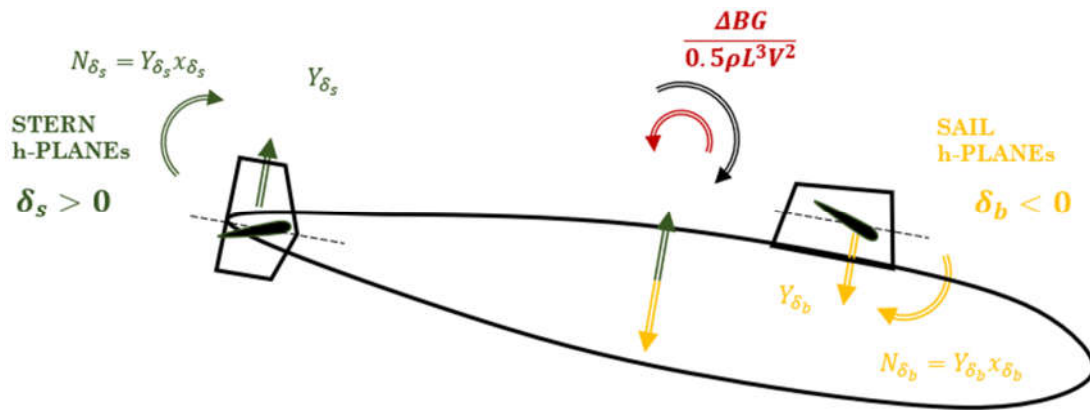


Figure A1. Meander test forces.

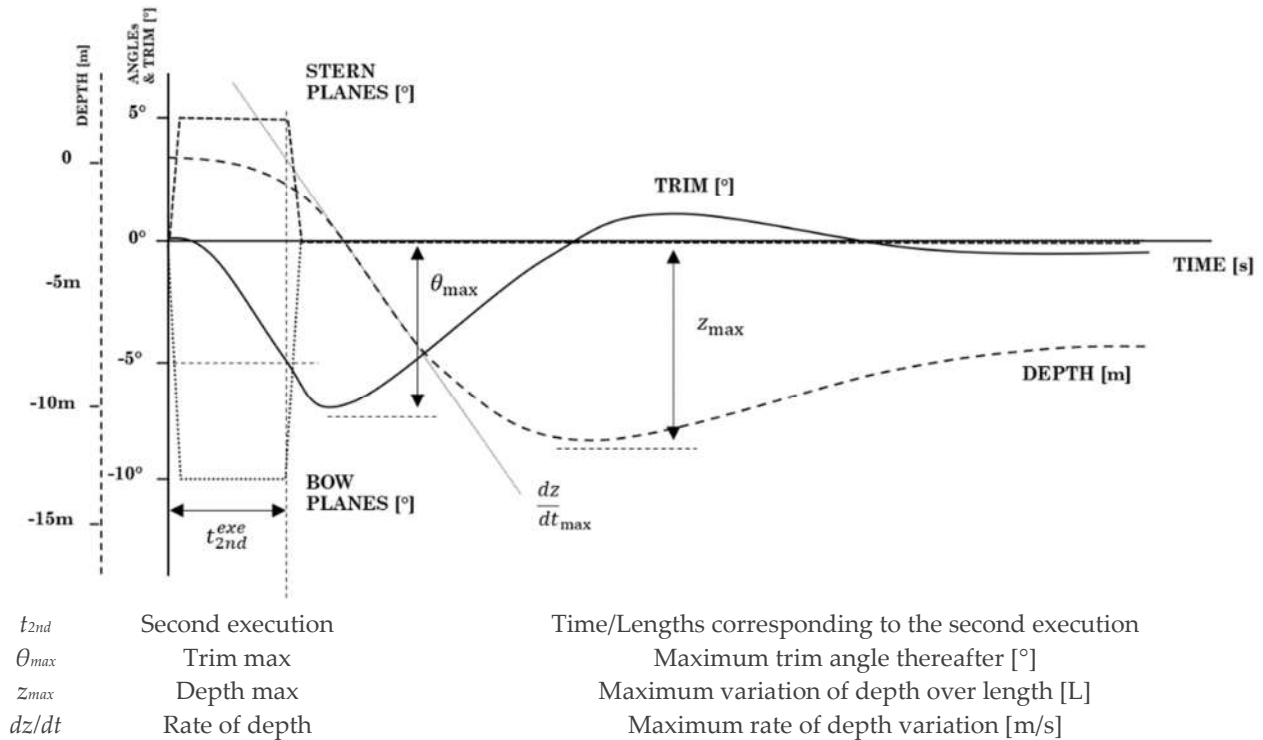
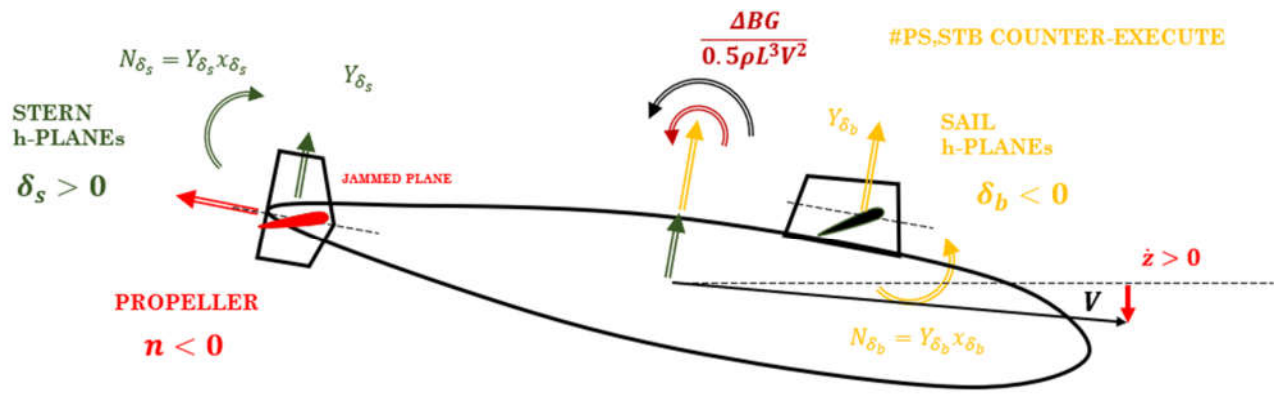


Figure A2. Meander test time-series and characteristics.

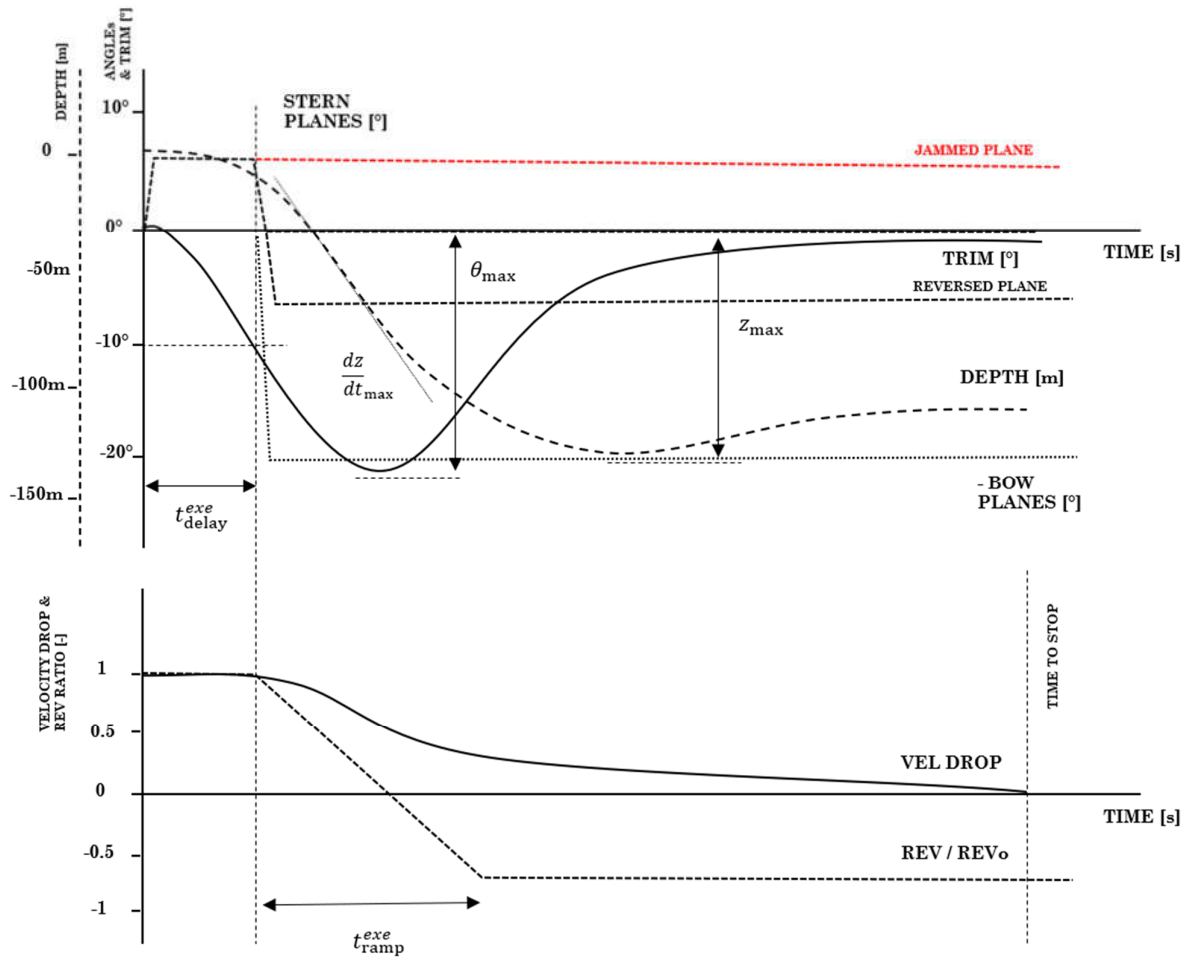
Appendix A.2. Dive Fail Test

The dive fail test is a variation of the Meander test and is executed by jamming the stern planes in the descent direction at the second execution and crash stopping: Starting from this moment, the bow planes are flipped to compensate the bow upwards, and with a delay of 15 s, the thrust is reversed at -70% of revolutions with a ramp of 60 s—see Figure A3. The emergency manoeuvre is called “DFs5b10n7_15s60s”, and the summarising parameters reported in the histograms are the maximum trim angle, the head reach in the longitudinal direction, and the depth change vertically to stop. The philosophical rational concerns the attitude safety assessment and the allowance depth band evaluation in case of emergency to avoid emerging or overtaking the structural collapse depth. The additional characteristic quantities are reported in the table and timeseries of Figure A4.



#2,4 JAMMED DIVING
if possible, the second not jammed is reversed

Figure A3. Dive fail forces.



θ_{max}	Trim max	Maximum trim angle thereafter [°]
X_{max}	Head reach	Longitudinal extent to stop [L]
Y_{max}	Lateral deviation	Transverse extent to stop [L]
Z_{max}	Depth deviation	Vertical extent to stop [L]

Figure A4. Dive fail time-series and characteristics.

Appendix B

Linear Stability Indexes

In the following lines, a summary and analysis of the linear stability properties of the vehicles are reported, in particular: the horizontal stability index G_h , the vertical stability index G_v , the damping ratio DR at two velocities, the stern planes critical velocity V_c , and the lower vertical stability velocity threshold $V_{re>0}$ in the case of unstable vehicles—for complete definitions see Feldman (1979).

The **horizontal stability** index is defined according to the following:

$$G_h = 1 - \frac{b_v}{b_r} > 0$$

where

$$b'_v = \frac{N'_v}{Y'_v} \text{ h-drift destabilising lever}$$

$$b'_r = \frac{N'_r - m'x'_g}{Y_r - m'} \text{ yaw stabilising lever}$$

The **vertical stability** index at high-speed under the assumption that the hydrodynamic forces cancel out the restoring term is defined according to the following:

$$G_v = 1 - \frac{b_w}{b_q} > 0$$

where

$$b'_w = -\frac{M'_w}{Z'_w} \text{ v-drift destabilising lever (also called neutral point } x'_{NP})$$

$$b'_q = -\frac{M'_q - m'x'_g}{Z_q + m'} \text{ pitch stabilising lever}$$

The **neutral point** is the longitudinal coordinate where, if applied a vertical force, the vehicle will experience a direct vertical shift, i.e., a depth change without variation of attitude. Normally, bow planes are installed around this coordinate. At low speeds, this becomes fundamental when the depth control is lost due to the critical threshold of velocity trespass. This coordinate corresponds to the longitudinal centre of pressure of the vertical drift motion, i.e., the above v-drift destabilizing lever.

The **critical point**, vice versa, is the longitudinal coordinate according to where, if applied a force, the vehicle will only change trim attitude without varying the depth. This position relies on the comparison between hydrodynamic forces and restoring moment so that no resultant unbalanced vertical forces exist. The lower the velocity, the less effective the stern planes, and the more this point will shift astern. In terms of design, the **critical velocity** is identified when the critical point overlaps onto the stern control planes. This threshold velocity determines if the pitch moment caused by the control surface force will generate a trim and a sufficient vertical angle of attack to make the vehicle shift in the direction of the drift force (opposite to the control surface force) or will make drift the vehicle vertically in the direction of the control surface force (see Figure A5). The point can be located starting from the pitch equilibrium between hydrodynamic forces and restoring moment:

$$-\frac{\Delta BG}{0.5\rho L^3 V^2} \theta + Z'_w(x'_{NP} - x'_{CP}) \beta_v = 0$$

By imposing a horizontal course (neutral variation of depth), i.e., with a pitch angle θ identical and opposite to the vertical drift angle $-\beta_v$, the following quantities can be evaluated by once varying the velocity for obtaining the critical point position, and then, by setting the critical point at the stern planes for obtaining the critical velocity of the current design:

$$x'_{CP} = x'_{NP} + \frac{\Delta BG}{0.5\rho L^3 V^2 Z'_w} \text{ Critical point (also called trim point)}$$

$$V_c = \sqrt{\frac{\Delta BG}{0.5\rho L^3 Z'_w(x'_{NP} - x'_{CP})}} \text{ Critical velocity}$$

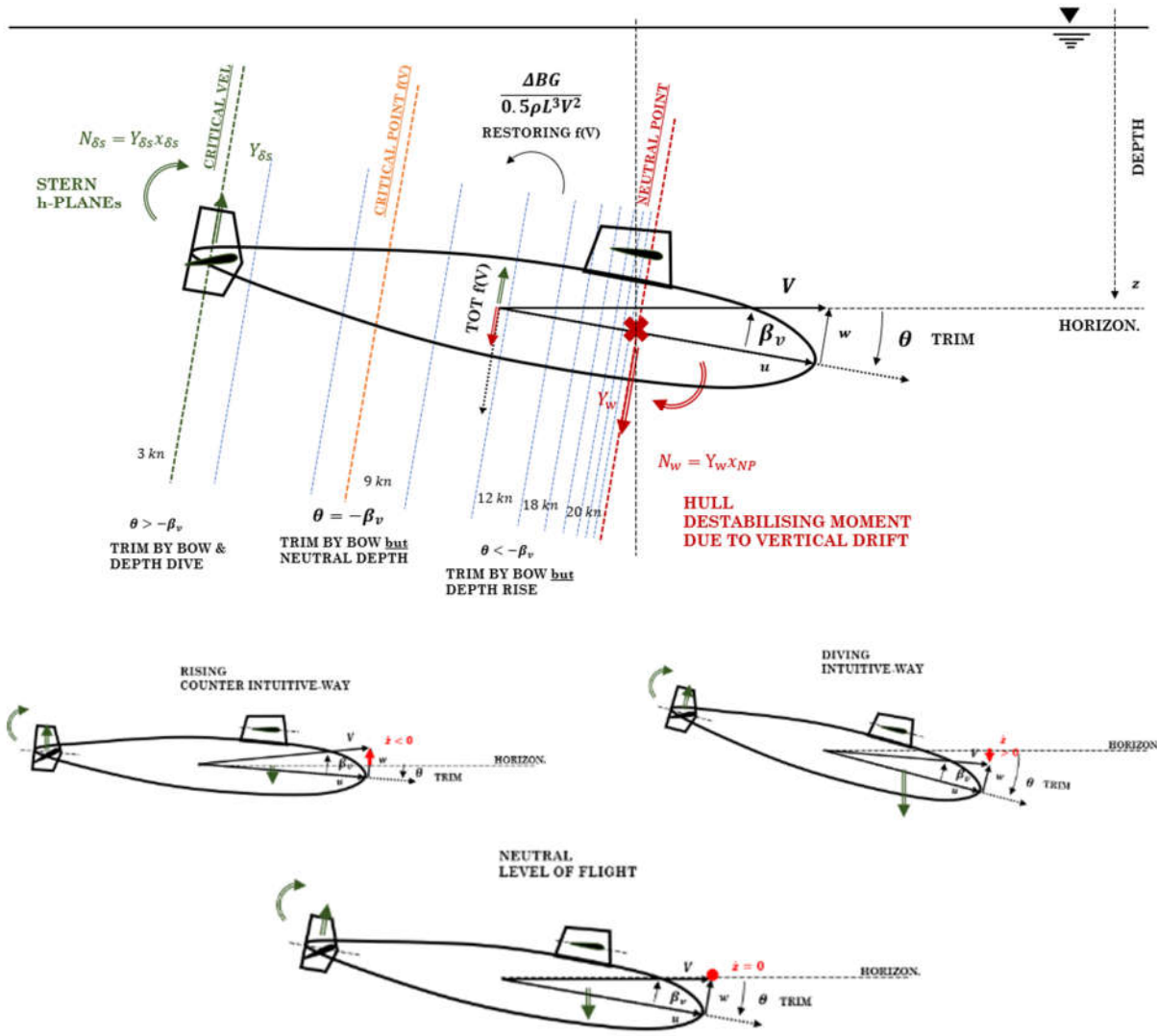


Figure A5. Depth change ability due to stern planes execution—critical point and velocity.

Finally, the **damping ratio** is a nondimensional index of the oscillations decaying factor on the vertical plane due to any disturbance around the equilibrium point of straight sailing. The definition follows standard dynamic system equations written in normal form in the fashion of damped harmonic oscillators by defining the natural frequencies, the critical damping, and the damping ratio. The damping ratio will rely on the vehicle velocity.

As a general remark, Feldman and Gertler suggest the following parameter for a good design both stable and prompt in dynamic response: (i) $G_h > 0$, about 0.2 (marginally stable); (ii) $G_v > 0$; (iii) $DR \sim 0.7$ at moderate speed; $DR > 1$ at high speed; $DR \sim 0.2$ at low speed.

The SMG design: As an example, Table A1 summarises the linear stability properties of the original SMG used as the reference design for the study. The fidelity of the modelling is substantial. Both the stability indexes and the critical velocities are substantially caught by the modelling. The vehicle is marginally stable on the horizontal plane while supplying a greater margin onto the vertical plane to best cope with the speed effect. As an example, Figure A6 depicts the SMG vertical damping ratio trend with velocity obtained from the simulation model, which is typical of modern submarines: the

experiments positively remark a value of 0.75 at 10 kn with BG = 0.27m. The critical velocity is well matched around 3.5 kn.

Table A1. Linear stability indexes validation.

		SMG	
		EXP	MODEL
Gh		0.10	0.06
Gv		0.81	0.67
DR	5 kn		0.58
	10 kn	0.75	0.72
Vc		3.50	3.10

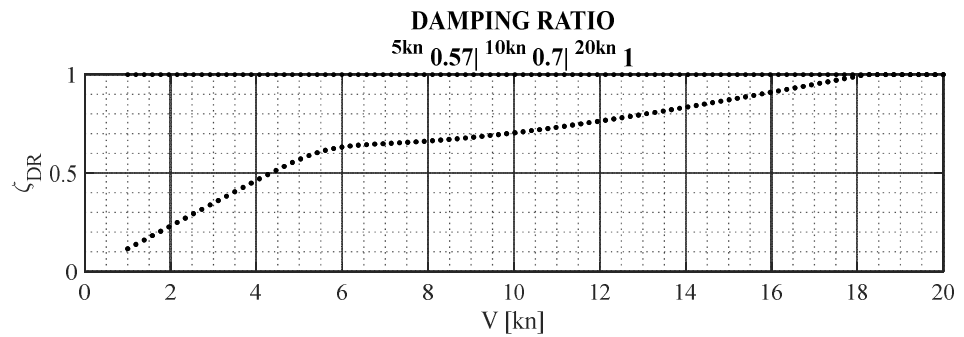
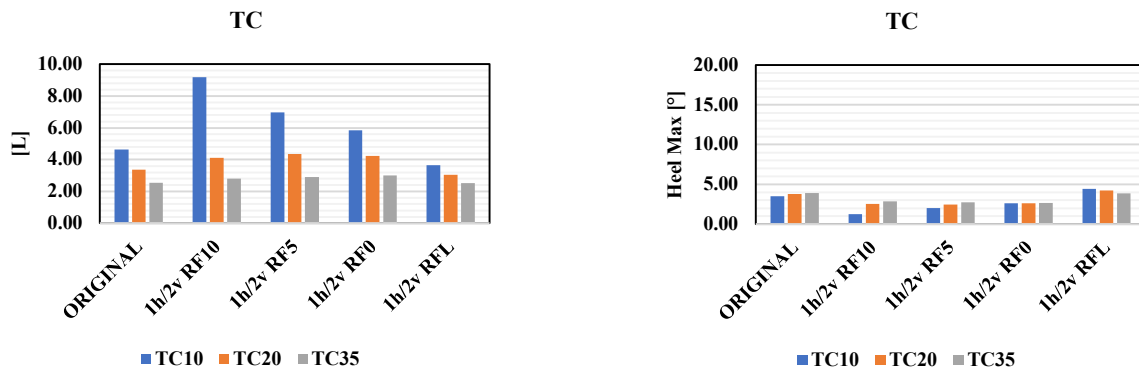


Figure A6. SMG—Damping ratio.

Appendix C

Manoeuvring Failure Modes

Figures A7 and A8 depict the full results of the +-setup and x-setup designs in the degraded conditions.



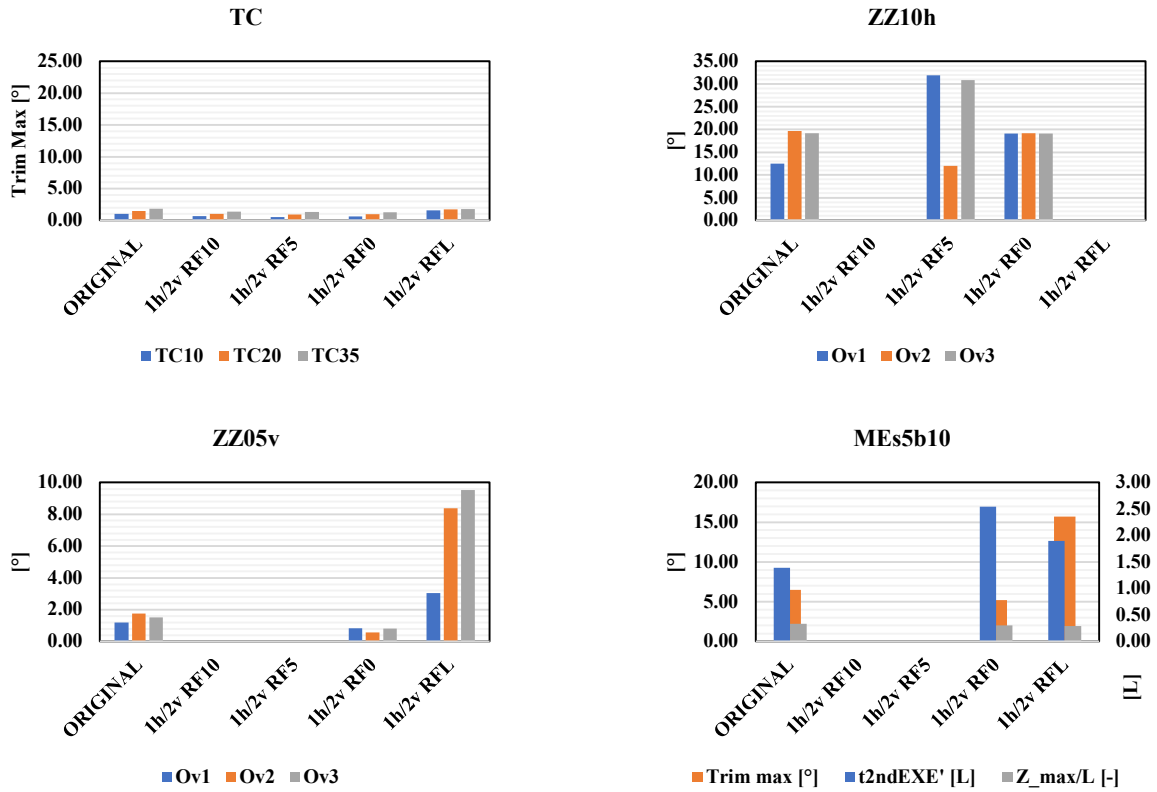
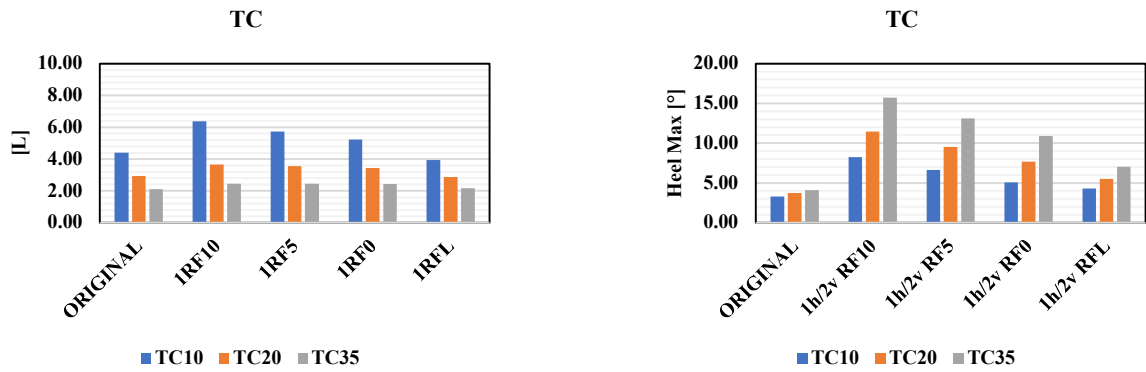


Figure A7. SMG +Eq Failures.



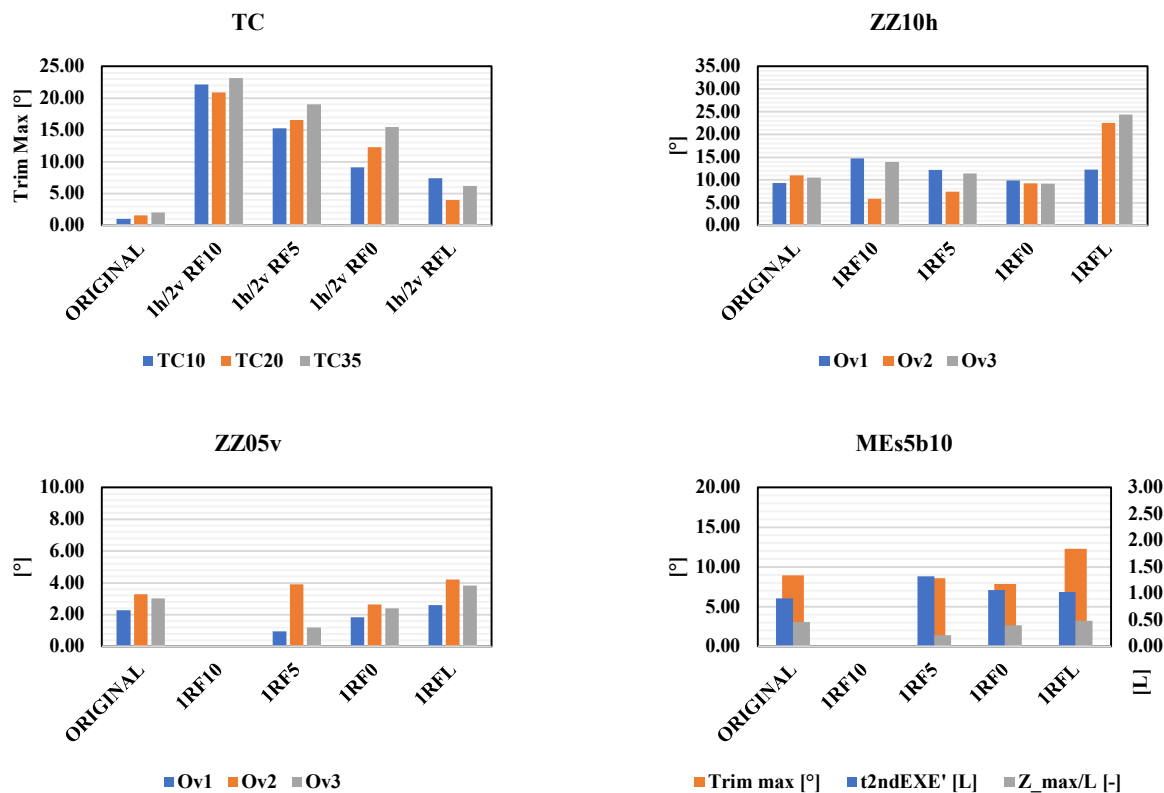


Figure A8. SMG x-Eq Failures.

References

1. Abkowitz, M. *Lectures on Ship Hydrodynamics—Steering and Maneuvering*; Hydro-and Aerodynamics Laboratory Report (Hy-5); Hydro & Aerodynamic Laboratory: Lyngby, Denmark, 1964.
2. Ankudinov, V.; Kaplan, P.; Jacobsen, B. Assessment and principal structure of the modular mathematical model for ship maneuverability predictions and real-time maneuvering simulation. In Proceedings of the MARSIM'93, International Conference on Marine Simulation and Ship Manoeuvrability, International Marine Simulator Forum (IMSF), St. John's, NL, Canada, 26 September–2 October 1993.
3. Hooft, J.P.; Nienhuis, U.; Hutchison, B.L.; Daidola, J.C.; Jakobsen, B.K.; Ankudinov, V. The prediction of the ship's maneuverability in the design stage. *Trans. Soc. Naval Archit. Mar. Eng.* **1994**, *102*, 419–445.
4. Oltmann, P.; Sharma, S. *Simulation of Combined Engine and Rudder Manoeuvres Using an Improved Model of Hull-Propeller-Rudder Interactions*; Technical University: Hamburg, Germany, 1984.
5. Sutulo, S.; Moreira, L.; Guedes Soares, C. Mathematical models for ship path prediction in manoeuvring simulation systems. *Ocean. Eng.* **2002**, *29*, 1–19.
6. Carchen, A.; Turkmen, S.; Piaggio, B.; Shi, W.; Sasaki, N.; Atlar, M. Investigation of the manoeuvrability characteristics of a Gate Rudder system using numerical, experimental, and full-scale techniques. *Appl. Ocean Res.* **2020**, *106*, 102419. <https://doi.org/10.1016/j.apor.2020.102419>.
7. Dubbioso, G.; Viviani, M. Aspects of twin screw ships semi-empirical maneuvering models. *Ocean. Eng.* **2012**, *48*, 69–80.
8. Viviani, M.; Martelli, M.; Vignolo, S.; Altosole, M.; Figari, M. Numerical modelling of propulsion, control and ship motions in 6 degrees of freedom. *Proc. Inst. Mech. Eng. Part M J. Eng. Marit. Environ.* **2014**, *228*, 373–397.
9. Franceschi, A.; Piaggio, B.; Tonelli, R.; Villa, D.; Viviani, M. Assessment of the manoeuvrability characteristics of a twin shaft naval vessel using an open-source cfd code. *J. Mar. Sci. Eng.* **2021**, *9*, 665.
10. Franceschi, A.; Piaggio, B.; Villa, D.; Viviani, M. Development and assessment of CFD methods to calculate propeller and hull impact on the rudder inflow for a twin-screw ship. *Appl. Ocean Res.* **2022**, *125*, 103227.
11. Piaggio, B.; Franceschi, A.; Villa, D.; Ferrari, V.; Tonelli, R.; Viviani, M. The heel influence on ship manoeuvrability: Single and twin-screw surface vessels. *Ocean. Eng.* **2022**, *266*, 112721.
12. Woodward, M.; Atlar, M.; Clarke, D. Application of the IMO Maneuvering Criteria for Pod-Driven Ships. *J. Ship Res.* **2009**, *53*, 106–120.

13. Yeon-Gyu, K.; Kun-Hang, Y.; Sun-Young, K.; Nam-Sun, S. Study of a Characteristics of Maneuvering Mathematical Model of Twin POD Cruise Ship. *J. Soc. Nav. Archit. Korea* **2013**, *50*, 429–435.
14. Piaggio, B.; Villa, D.; Viviani, M. Twin-screw vessel manoeuvrability: The traditional twin-rudder configuration vs pod-drives. *Ocean. Eng.* **2022**, under final review.
15. Figari, M.; Martinelli, L.; Piaggio, B.; Enoizi, L.; Viviani, M.; Villa, D. An all-round design-to-simulation approach of a new Z-drive escort tug class. *J. Offshore Mech. Arct. Eng.* **2020**, *142*, 031107.
16. Jiang, T.; Henn, R.; Sharma, S.D. Dynamic behavior of a tow system under an autopilot on the tug. In Proceedings of the International Symposium and Workshop on Forces Acting on a Manoeuvring Vessel MAN'98, Val de Reuil, France, 16–18 September 1998.
17. Piaggio, B.; Viviani, M.; Martelli, M.; Figari, M. Z-Drive Escort Tug manoeuvrability model and simulation, Part II: A full-scale validation. *Ocean. Eng.* **2022**, *259*, 111881.
18. Xu, H.T.; Hassani, V.; Guedes Soares, C. Truncated least square support vector machine for parameter estimation of a nonlinear manoeuvring model based on PMM tests. *Appl. Ocean Res.* **2020**, *97*, 102076.
19. Serge, S.; Guedes Soares, C. An algorithm for offline identification of ship manoeuvring mathematical models from free-running tests. *Ocean. Eng.* **2014**, *79*, 10–25.
20. Perera, L.P.; Ferrari, V.; Santos, F.P.; Hinostroza, M.A.; Guedes Soares, C. Experimental Evaluations on Ship Autonomous Navigation and Collision Avoidance by Intelligent Guidance. *IEEE J. Ocean. Eng.* **2015**, *40*, 374–387.
21. Bonci, M.; Viviani, M.; Broglio, R.; Dubbioso, G. Method for estimating parameters of practical ship manoeuvring models based on the combination of RANSE computations and System Identification. *Appl. Ocean. Res.* **2015**, *52*, 274–294.
22. Kose, K. On a new mathematical model of maneuvering motions of a ship and its applications. *Int. Shipbuild. Prog.* **1982**, *29*, 205–220.
23. Ogawa, A.; Kasai, H. On the mathematical model of manoeuvring motion of ships. *Int. Shipbuild. Prog.* **1978**, *25*, 306–319.
24. Sutulo, S.; Guedes Soares, C. Review on Ship Manoeuvrability Criteria and Standards. *J. Mar. Sci. Eng.* **2021**, *9*, 904.
25. Munk, M. *The Aerodynamic Forces on Airship Hulls*; Report 184; National Advisory Committee for Aeronautics: Washington, DC, USA, 1924.
26. Lambert, J.D. *The Effect of Changes in the Stability Derivatives on the Dynamic Behaviour of a Torpedo*; Aeronautical Research Council Reports and Memoranda 1956, No 3143; Admiralty Research Laboratory: London, UK: 1956.
27. Hoyt, E.D.; Imlay, F.H. *The Influence of Metacentric Stability on the Dynamic Longitudinal Stability of a Submarine*; Report C-158; David Taylor Model Basin: Washington, DC, USA, 1948.
28. Pattison, D.R. *Stability and Control of Submarines: A Review of Design Criteria and Derivative Prediction Techniques*; AEW Report no 7/75; Procurement Executive Ministry of Defence: Haslar, UK, 1975.
29. Pitts, W.C.; Nielsen, J.N.; Kaattari, G.E. *Lift and Center of Pressure of Wing-Body-Tail Combinations at Subsonic, Transonic, and Supersonic Speeds*; Report 1307; National Advisory Committee for Aeronautics: Washington, DC, USA, 1959.
30. Feldman, J.P. *DTNSRDC Revised Standard Equations of Motion*; DTNSRDC/SPD-0393-09; David Taylor Naval Ship Research and Development Center: Potomac, MD, USA, 1979.
31. Feldman, J.P. *Method of Performing Captive-Model Experiments to Predict the Stability and Control Characteristics of Submarines*; CRDKNSWC-HD-0393-25; Carderock Division Naval Surface Warfare Center: Bethesda, MD, USA, 1995.
32. Bohlmann, H.J. *Berechnung hydrodynamischer Koeffizienten von Ubooten zur Vorhersage des Bewegungsverhaltens*; Technische Universität Hamburg: Harburg, Germany, 1990.
33. Toxopeus, S. Viscous-flow calculations for bare hull DARPA SUBOFF submarine at incidence. *Int. Shipbuild. Prog.* **2008**, *55*, 227–251.
34. Yong, J.C.; Woochan, S.; Ki-Hyeon, C.; Shin, H.R. Maneuvering simulation of an X-plane submarine using computational fluid dynamics. *Int. J. Nav. Archit. Ocean. Eng.* **2020**, *12*, 843–855.
35. Lin, Y.H.; Tseng, S.H.; Chen, Y.H. The experimental study on maneuvering derivatives of a submerged body SUBOFF by implementing the Planar Motion Mechanism tests. *Ocean. Eng.* **2018**, *170*, 120–135.
36. Bettle, M.C. *Validating Design Methods for Sizing Submarine Tailfins*; Naval Submarines and UUV's, Papers; RINA, Royal Institution of Naval Architects—Warship: Bath, UK, 2014; pp. 133–146.
37. Gaggero, S.; Piaggio, B.; Vernengo, G.; Villa, D.; Viviani, M.; Gualeni, P. Numerical Approaches for Submarine Hydrodynamic Design and Performance Analysis. *Prog. Mar. Sci. Technol.* **2022**, *6*, 279–286.
38. Dempsey, E.M. *Static Stability Characteristics of a Systematic Series of Stern Control Surfaces on a Body of Revolution*; Report 77-0085; DTNSRDC, David and Taylor Naval Ship Research and Development Center: Bethesda MD, USA, 1997.
39. Mackay, M.; Bohlmann, H.J.; Watt, G.D. Modelling submarine tailplane efficiency. In *Challenges in Dynamics, System Identification Control and Handling Qualities for Land, Air, Sea, and Space Vehicles (RTO-MP-095)*; NATO RTO: Washington, DC, USA, 2002.
40. Lee, S.K.; Manovski, P.; Kumar, C. Wake of a cruciform appendage on a generic submarine at 10° yaw. *J. Mar. Sci. Technol.* **2020**, *25*, 787–799.
41. Carrica, P.M.; Kerkvliet, M.; Quadvlieg, F.; Ezequiel, J.M. CFD Simulations and Experiments of a Submarine in Turn, Zigzag, and Surfacing Maneuvers. *J. Ship Res.* **2021**, *65*, 293–308.
42. Toxopeus, S.; Kerkvliet, M.; Vogels, R.; Quadvlieg, F.; Nienhuis, B. Submarine hydrodynamics for off-design conditions. *J. Ocean. Eng. Mar. Energy* **2020**, *8*, 499–511.
43. Dubbioso, G.; Broglio, R.; Zaghi, S. CFD analysis of turning abilities of a submarine model. *Ocean. Eng.* **2017**, *129*, 459–479.

44. Zaghi, S.; Dubbioso, G.; Broglia, R.; Cannarozzo, M. Virtual PMM and free running manoeuvring predictions of a submarine by CFD. In Proceedings of the NAV 2015 18th International Conference on Ships and Shipping Research, Lecco, Italy, 24–26 June 2015.
45. Watt, G.D. *Modelling and Simulating Unsteady Six Degrees-of-Freedom Submarine Rising Maneuvers*; Tech. Rep. 2007; Defence Research and Development Canada: Ottawa, ON, Canada, 2007.
46. Skejic, R.; Faltinsen, O. Maneuvering of submarines at periscope depths in a seaway. In Proceedings of the 15th International Symposium on Practical Design of Ships and Other Floating Structures, PRADS 2022, Dubrovnik, Croatia, 9–13 October 2022.
47. Furlong, M. System Identification of the Hydrodynamic Characteristics of Underwater Vehicles. Ph.D Thesis, University of Southampton, Southampton, UK, 2005.
48. Xu, H.T.; Hassani, V.; Guedes Soares, C. Comparing generic and vectorial nonlinear manoeuvring models and parameter estimation using optimal truncated least square support vector machine. *Appl. Ocean Res.* **2020**, *97*, 102061.
49. Roddy, R.F. *Investigation of the Stability and Control Characteristics of Several Configurations of the DARPA Suboff Model (DTRC Model 5470) from Captive-Model Experiments*; David Taylor Research Center: Bethesda, MD, USA, 1990.
50. Overpelt, B.; Nienhuis, B.; Anderson, B. Free running manoeuvring model tests on a modern generic SSK class submarine (BB2). In Proceedings of the Pacific International Maritime Conference, Sydney, Australia, 6–8 October 2015.
51. Mojtaba, M.A.; Esperança, P.; Vitola, M.; Sphaier, S. An initial evaluation of the free surface effect on the maneuverability of underwater vehicles. *Ocean. Eng.* **2020**, *196*, 106851.
52. Nascimento, E.G.; Tannuri, E.A. Development of a submarine maneuvering simulator. In Proceedings of the Warship, Future Technologies in Naval Submarines, London, UK, 2–3 June 2021.
53. Thuné, S. Simulation of Submarine Manoeuvring. Master's Thesis, Royal Institute of Technology Sweden, Stockholm, Sweden, 2015.
54. Clarke, D. Paper 8. A Two-Dimensional Strip Method for Surface Ship Hull Derivatives: Comparison of theory with Experiments on a Segmented Tanker Model. *J. Mech. Eng. Sci.* **1972**, *14*, 53–61.
55. Toxopeus, S. Validation of slender-body method for prediction of linear manoeuvring coefficients using experiments and viscous-flow calculations. In Proceedings of the 7th International Conference on Hydrodynamics, Ischia, Italy, 2006; pp. 589–598.
56. Mazzarello, G. *Teoria Utilizzata nel Programma "Dimiton" per il Calcolo Della Stabilità Dinamica e Della Manovrabilità di un Sottomarino*; Fincantieri Internal Report; ITA: Genoa, Italy, 1996; Volumes 1–2.
57. Whicker, L.F.; Fehlner, L.F. *Free Stream Characteristics of a Family of Low Aspect Ratio Control Surfaces for Application to Ship Design*; DTMB Report 933; David Taylor Model Basin: Washington, DC, USA, 1958.
58. Windsor, R.I. *Survey of Low Aspect Ratio Characteristics Useful in the Design of Control Surfaces*; Wind Tunnel Report 62-1; University of Maryland: College Park, MD, USA, 1962.
59. Thieme, H. *Design of Ship Rudders, DTRC, 1965, Translation No.321. Original Version "Zur Formgebung von Schiffsrudern" Schriftenreihe Schiffbau*; TUH: Hamburg, Germany, 1962.
60. Molland, A.F.; Turnock, S. *Marine Rudders and Control Surfaces. Principles, Data, Design and Applications*; Butterworth-Heinemann: Oxford, UK; Elsevier: Amsterdam, The Netherlands, 2007.
61. Lyons, D.J.; Bisgood, P.L. *An Analysis of the Lift Slope of Aerofoils of Small Aspect Ratio, including Fins, with Design Charts for Aerofoils and Control Surfaces*; Aeronautical Research Council Reports and Memoranda, No 2308; Ministry of Supply: London, UK, 1945.
62. Kerwin, J.E.; Mandel, P.; Lewis, S.D. An experimental study of series of flapped rudders. *J. Ship Res.* **1972**, *16*, 221–239.
63. Kerwin, J.E.; Lewis, S.D.; Oppenheim, B.W. *Experiments on Rudders with Small Flaps in Free Stream and behind a Propeller*; Report no 74-16; Department of Ocean Engineering, Massachusetts Institute of Technology: Cambridge, MA, USA, 1974.
64. Harris, R.G. *Forces on a Propeller Due to Sideslip*; ARC R & M 427; Reports and Memoranda, No. 427; British Aeronautical Research Council: London, UK, 1918.
65. Dubbioso, G.; Muscari, R.; Di Mascio, A. Analysis of the performances of a marine propeller operating in oblique flow. *Comput. Fluids* **2013**, *75*, 86–102.